Zeitschrift für Kristallographie 155, 81–113 (1981)


# The crystal chemistry of ($Mn^{3+}$, $Fe^{3+}$)-substituted andalusites (viridines and kanonaite), $(Al_{1-x-y}Mn_x^{3+}Fe_y^{3+})_2$ $(O|SiO_4)$: crystal structure refinements, Mössbauer, and polarized optical absorption spectra

I. Abs-Wurmbach,

Institut für Mineralogie, Universität Bochum,
D-4630 Bochum, Federal Republic of Germany*

K. Langer,

Institut für Mineralogie und Kristallographie, Technische Universität Berlin,
D-1000 Berlin

F. Seifert,

Mineralogisches Institut, Universität Kiel,
D-2300 Kiel, Federal Republic of Germany

and E. Tillmanns

Institut für Geowissenschaften, Universität Mainz,
D-6500 Mainz, Federal Republic of Germany

Received: April 3, 1980

**Abstract.** The crystal chemistry of viridines and kanonaite, $(Al_{1-x-y}Mn_x^{3+}\ Fe_y^{3+})_2$ $(O|SiO_4)$, has been evaluated with special reference to the behavior of $Mn^{3+}$ in this andalusite type structure. Five natural samples (from Ultevis: $x = 0.012$, $y = 0.028$; from Yakutia: $x = 0.076$, $y = 0.046$; from Tanzania: $x = 0.091$, $y = 0.031$; from Darmstadt: $x = 0.171$, $y = 0.048$; from Kanona: $x = 0.340$, $y = 0.009$) and two synthetic viridines ($P135$: $x = 0.173$, $y = 0.005$; $P150$: $x = 0.22$, $y = 0$) have been studied by means of X-ray powder diffraction, single crystal-structure refinements, $^{57}Fe$ $\gamma$-resonance spectroscopy, and optical absorption microspectroscopy.

The structure refinements reveal that the transition metal ions substitute for Al almost exclusively in the distorted octahedral Al(1) site of the andalusite structure type within the entire mixed crystal series. This is independently proven by the Mössbauer results for $^{57}Fe$, which show that only 10 to 15% of total iron is present in the Al(2) trigonal-bipyramidal site. With increasing substitution, the octahedral $(c/a)_{oct}$ ratio increases. This

* Present address: Mineralisch-petrographisches Institut, Universität Bern, CH-3012 Bern, Switzerland

result is corroborated by the increasing energy of the $Mn^{3+}$ $^5B_{1g} \rightarrow {}^5A_{1g}$ transition as determined from the optical spectra. The increasing octahedral elongation leads to a tilting of both the $Al(2)O_5$ trigonal bipyramids and $SiO_4$ tetrahedra, and to slight changes of several of the Al(2)−O bond distances. These changes, although similar to those observed at high temperatures (Winter and Ghose, 1979), are considerably stronger than those caused by high temperature (e.g., $\Delta(c/a)_{oct}/(c/a)_{oct}$ to be extrapolated for $x = 0.5$ is approximately 0.1 while at 1000°C this relative change is only 0.035]. In the optical spectra, spin-allowed and spin-forbidden transitions of $Mn^{3+}$ are identified near 15000 $cm^{-1}$ [$^5B_{1g} \rightarrow {}^5A_{1g}(D)$], 18000 $cm^{-1}$ {$^5B_{1g} \rightarrow [^3T_{1g}(H)]$}, 19700 $cm^{-1}$ {$^5B_{1g} \rightarrow [^3T_{1g}(H)]$}, 21800 $cm^{-1}$ [$^5B_{1g} \rightarrow {}^5B_{2g}(D)$], 23300 $cm^{-1}$ [$^5B_{1g} \rightarrow {}^5E_g(D)$] and spin forbidden $Fe^{3+}$ transitions near 19700 $cm^{-1}$ {$^6A_{1g} \rightarrow [^4T_{2g}(G)]$}, 20800 $cm^{-1}$ {$^6A_{1g} \rightarrow [^4T_{2g}(G)]$}, 22300 $cm^{-1}$ {$^6A_{1g} \rightarrow [^4A_{1g}, {}^4E_g](G)$}, 23300 $cm^{-1}$ {$^6A_{1g} \rightarrow [^4A_{1g}, {}^4E_g](G)$}. The crystal-field parameter 10 $Dq$ for $Mn^{3+}$ decreases in the whole series by approximately 10%. However, this effect is compensated by increasing groundstate splitting such that the crystal field stabilazation energy of $Mn^{3+}$ is nearly constant, $198 \pm 2$ kJ/g-atom $Mn^{3+}$, in the whole range of solid solutions, $0.0 \leqq x \leqq 0.4$, which were studied.

## 1. Introduction

The aluminium silicates, andalusite, sillimanite, and kyanite, play a prominent role in metamorphic petrology and in the ceramic and material sciences. Therefore their crystal chemistry has been studied by numerous investigators (e.g., Burnham and Buerger, 1961; Burnham 1963a and b; Holuj et al., 1966; Chinner et al., 1969; Strens, 1968; Faye and Nickel, 1969; Faye and Harris, 1969; Smith and Strens, 1976; Langer, 1976, and authors in the legend of Fig. 1). Their work includes 3 $d$ transition-metal ion substitutions for Al, the partition behavior of the 3 $d$ ions between the different polymorphs, and the influence of such substitutions on the thermodynamic and physical properties of the respective minerals.

One of the results of the above crystallochemical and geochemical research was that manganese may be incorporated in the andalusite structure type in large amounts (Fig. 1), while in natural sillimanites and kyanites only trace to minor amounts of this element may be present. Furthermore, the maximum iron contents in manganese-free andalusites (Fig. 1) do not greatly exceed those of sillimanites and kyanites while, in combination with manganese, the iron contents may be appreciably higher (Fig. 1). The PT-stability range of the andalusite-type phase is greatly enlarged by manganese substitutions compared with the pure $Al_2[O|SiO_4]$-polymorph as evident from experimental work (Abs-Wurmbach et al., 1980).

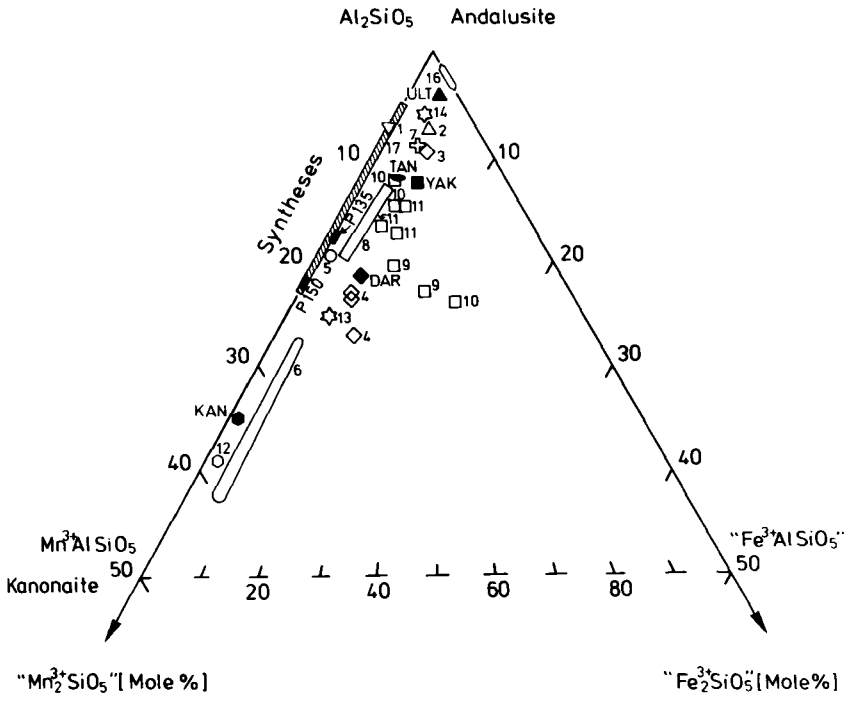


**Fig. 1.** Composition of natural $Mn^{3+}$, $Fe^{3+}$-, and synthetic $Mn^{3+}$-bearing andalusite type minerals (viridines and kanonaites). Localities are designated by different symbols, where closed and open ones refer to samples studied in the present paper (Table 1) or to literature data, respectively. Symbols used: ▽ Vestanä/Sweden, △ Ultevis/Sweden, ◇ Darmstadt/Germany, ○ or ⬭ Salm Château/Belgium, ✚ Kiawa Mountain/New Mexico USA, ▭ Hidaka Mountains/Hokkaido Japan, □ South Yakutia/Siberia USSR, ⬡ Kanona/Zambia, ✡ Central and Western Australia, ⬭ Mhwana/Tanzania, ⬭ Steinach/Germany, ▧ synthetic viridines. Numbers beside the symbols refer to the respective literature from which the analytical data were taken (1. Bäckström, 1896; 2. Ödmann, 1950; 3. Klemm, 1911; 4. Abraham and Schreyer, 1975; 5. Kramm, 1973; 6. Kramm, 1979; 7. Heinrich and Corey, 1959; 8. Grapes and Hashimoto, 1977; 9. Serdyuchenko, 1949; 10. Kulish, 1961; 11. K. Abraham, personal communication; 12. Vrána et al., 1978; 13. S. Hill, personal communication 1977; 14. Prider, 1960; 15. Meinhold and Frisch, 1970; 16. Okrusch and Evans, 1970; 17. Abs-Wurmbach et al., 1979)

A crystallochemical study of andalusites containing Mn and Fe was thus necessary to elaborate the basis for an explanation of these observations. Such a study is undertaken in the present paper by means of techniques including structure refinements and spectroscopy in order to determine the behavior of manganese and iron in the andalusite structure. The aim is to evaluat the crystallochemical properties as a function of the degree of the Mn and Fe substitutions.

Optical spectra of andalusites containing Mn and Fe (viridine[1]) taken in the visible range were presented as early as 1934 by Corin and 1948 by Shabynin. Shabynin (1948) concluded from his spectra that manganese should be divalent, which would require incorporation of equivalent amounts of protons for charge balance. This interpretation was rejected by later spectral work (Abs-Wurmbach et al., 1977; Hålenius, 1978), which permits the conclusion that both $3d$ elements are present in the trivalent state. However, this later work has left open questions concerning the concentration dependence of spectral parameters and the role of $Fe^{3+}$ *dd* transitions in the spectra obtained.

This paper presents, therefore, structural and spectroscopic results for a series of natural andalusite-type minerals containing $Mn^{3+}$ and $Fe^{3+}$, including the new Mn-rich kanonaite, and for synthetic iron-free andalusites containing $Mn^{3+}$. The latter synthetic samples provide the possibility to identify $Fe^{3+}$ bands in the natural $Mn^{3+}$, $Fe^{3+}$ members containing $Fe^{3+}$ in addition to $Mn^{3+}$.

## 2. Experimental

### *Samples*

The natural and synthetic mineral samples studied are light to deep green, almost black, and strongly pleochroic with $X$ and $Z$ yellowish green and $Y$ emerald green. Source, composition, and lattice constants are summarized in Table 1[2].

### *X-ray diffraction*

Manganese bearing andalusites (viridines and kanonaite) are orthorhombic, space group *Pnnm*, as is the pure aluminum end member, andalusite. Space group *Pnnm* had already been used in the first structure determination of andalusite (Taylor, 1929).

Lattice constants of the synthetic viridines were determined by the Guinier method using $CuK\alpha_1$ radiation ($\lambda = 0.154051$ nm) and silicon

[1] Klemm (1911) introduced the name viridine for bright green Mn-bearing andalusites a name which has been well-established in the literature since that time. However, following a proposal of S. Vrána, who discovered an andalusite-type mineral exceptionally rich in Mn (Vrána et al., 1978), the Commission on New Minerals and Mineral Names of the IMA has deleted the name viridine, and suggested the name kanonaite for the end member $Mn^{3+}Al[O|SiO_4]$. According to the decision of the Commission, andalusites with $x < 0.25$ $Mn^{3+}$ (less than 50 mole % kanonaite) should be called manganian andalusite, those with $x > 0.25$ $Mn^{3+}$ (more than 50 mole % kanonaite) aluminous kanonaite

[2] Some results on the samples ULT and DAR have recently been published in a short communication (Abs-Wurmbach et al., 1977). In this paper the locality of the Ultevis viridine was erroneously called 'Laisvall'. Also, due to a typing error, wrong $y$ values were quoted for ULT and DAR in the paper referred to, and should be replaced by the values given in this paper

($a_0 = 0.54305$ nm) as an internal standard. The measurements were indexed and refined by a program written by Evans et al. (1963). Cell parameters of natural samples (Table 1) were determined from single crystals and refined by a least-squares fit to the angular settings of large-angle reflections ($\theta > 20°$) on an automatic four-circle diffractometer, using Mo$K\alpha_1$ radiation ($\lambda = 0.070926$ nm). Lattice constants of some natural samples were also determined by Guinier and diffractometer techniques.

Intensities were collected on the automated four-circle diffractometer using monochromatized Mo$K\alpha$ radiation (graphite monochromator) and the $\omega - 2\theta$ step-scan mode with a scan range of $\Delta\omega = 0.6 + 0.5 \tan\theta$. Conditions of measurements are summarized in Table 2. The diffracted-beam aperture was vertically constant and horizontally determined by $(4 + 2 \tan\theta)$ mm. The scanning speed was adjusted to obtain 5000 counts for each reflection with a maximum counting time of 180 s. The background was measured for one-quarter of the scan time on both sides of the peak. Possible crystal decomposition or change of orientation was controlled through three reference reflections monitored for intensity changes after every 60 measured reflections and after every 120 reflections for orientation changes. All four data sets were corrected for Lorentz, polarization and absorption effects; symmetrically equivalent structure factors were averaged. The crystal structures were refined by full-matrix least-squares calculations starting from the positional parameters of andalusite (Burnham and Buerger, 1961). Atomic scattering factors were obtained from Hamilton and Ibers (1974). For the $M1$ positions, a scattering factor curve was calculated from $f_{Al}$, $f_{Mn}$, and $f_{Fe}$. In these calculations, it was assumed that the amount of manganese and iron determined by microprobe (Table 1) occupies the $M1$ position only. This assumption was based on ionic-radius arguments and Mössbauer results (section 3), which show a strong concentration of iron in the $M1$ position. The weight of the observed structure factors was $w = 1/\sigma^2 F$. The computer programs used in the course of the work are the same as given by Tillmanns and Gebert (1973). Final $R$ values are shown in Table 2. The low values obtained confirm the above assumption for the $M1$ occupancy. Tables of observed and calculated structure factors can be obtained from the authors.

### *Mössbauer spectra*

The Mössbauer spectra were obtained on an Elscint Spectrometer operating in the constant acceleration mode using a $^{57}Co$ source in a rhodium matrix (activity 20 m Ci). Details of the experimental procedure are given in Seifert and Olesch (1977). Pure viridine concentrates were finely ground and baked to pellets, with absorber thicknesses generally ranging from 2 to 5 mg natural Fe per $cm^2$. The spectra were recorded with the absorbers held at temperatures of 77 and 298 K. Peaks of Lorentzian shape were fitted to the absorption envelope by a least-squares method.

**Table 1.** Source, composition, and lattice constants of $Mn^{3+}$-bearing natural and synthetic andalusite-type minerals studied, $(Al_{1-x-y}Mn_x^{3+}Fe_y^{3+})_2(O|SiO_4)$. Lattice constants were determined at room temperature (22 °C)

| Sample | AND | ULT | YAK | TAN | DAR | *P*135 | *P*150 | KAN |
|---|---|---|---|---|---|---|---|---|
| Source | Sta. Teresinha Mine/Brazil | Ultevis Sweden | Aldan Shield Yakutia USSR | Mhwana Tanzania | Darmstadt Germany | Synthetic (a) | Synthetic (a) | Kanona Zambia |
| Composition | | | | | | | | |
| Analytical method | wet chem. | EMP[b] | EMP[c] | EMP[d] | EMP[b] | EMP[b] | X-ray[e] | EMP[b] |
| No. of analyses | | | | | | | | |
| wt % | | 4 | 6 | | 2 | 8 | | 3 |
| $SiO_2$ | n. d. | 36.6(1) | 35.5(3) | | 34.3(2) | 34.2(6) | | 32.7(3) |
| $Al_2O_3$ | n. d. | 58.8(7) | 53.1(20) | | 44.0(4) | 48.2(11) | | 35.6(10) |
| $Mn_2O_3$ | < 0.01 | 1.11(4) | 7.1(18) | | 15.15(1) | 15.7(12) | | 29.1(7) |
| $Fe_2O_3$ | 0.40 | 2.72(4) | 4.3(4) | | 4.35(15) | 0.4(3) | | 0.82(5) |
| Total | | 99.23 | 100.04 | | 97.80 | 98.5 | | 98.22 |
| $x$ | < 0.0001 | 0.012 | 0.076 | 0.091 | 0.171 | 0.173 | 0.22 | 0.340 |
| $y$ | 0.004 | 0.028 | 0.046 | 0.031 | 0.048 | 0.005 | | 0.009 |

Lattice constants

| No. of reflections | 39[f] | 25[g] | 29[h]<br>28[g] | 33[h]<br>27[g] | 25[g] | 24[f] | 28[f] | 29[g] |
|---|---|---|---|---|---|---|---|---|
| $a$ [nm] | 0.7794(2) | 0.7810(2) | 0.7850(2)[h]<br>0.7839(2)[g] | 0.7841(2)[f]<br>0.7843(2)[g] | 0.7891(2) | 0.7891(3) | 0.7909(3) | 0.7961(2) |
| $b$ [nm] | 0.7899(2) | 0.7915(2) | 0.7944(2)[h]<br>0.7941(2)[g] | 0.7937(2)[f]<br>0.7944(2)[g] | 0.7988(2) | 0.7954(3) | 0.7975(5) | 0.8053(2) |
| $c$ [nm] | 0.5555(2) | 0.5570(2) | 0.5591(2)[h]<br>0.5582(2)[g] | 0.5579(1)[f]<br>0.5585(2)[g] | 0.5603(2) | 0.5583(1) | 0.5590(2) | 0.5616(2) |
| $V_o$ [$nm^3$] | 0.3420(2) | 0.3443(2) | 0.3486(1)[h] | 0.3472(1)[f]<br>0.3475(2)[g] | 0.3532(2)<br>0.3486(2)[g] | 0.3504(2) | 0.3525(2) | 0.3600(2) |

Numbers in brackets: uncertainty (1 s) in the last decimal point. EMP electron microprobe.
n. d. = Not determined

[a] Sysnthesis conditions cf. Abs-Wurmbach and Langer (1975)
[b] Analyst K. Abraham
[c] Analyst D. Ackermand
[d] After data from Meinhold and Frisch (1970)
[e] On the basis of the $V_o = f(x+y)$ plot (e) of Figure 2
[f,g,h] Lattice constants determined from Guinier, single crystal, diffractometer data, respectively.

**Table 2.** Experimental details: X-ray intensity measurement and refinement; conditions for measurement of the optical spectra

| | ULT | YAK | TAN | DAR | *P*135 | *P*150 | KAN |
|---|---|---|---|---|---|---|---|
| $\theta_{max}$ [degrees] | 30 | | 35 | 35 | | | 35 |
| Total number of measurements | 2196 | | 1745 | 3353 | | | 3404 |
| Number of unique reflections | 548 | | 825 | 841 | | | 857 |
| Reflections with $I < 2\sigma(I)$ | 13 | | 103 | 184 | | | 201 |
| $R_1 = \Sigma(\lvert F_o\rvert - \lvert F_c\rvert)/\Sigma\lvert F_o\rvert$ | 0.018 | | 0.019 | 0.032 | | | 0.041 |
| $R_2 = (\Sigma\omega[\lvert F_o\rvert - \lvert F_c\rvert]^2/\Sigma\omega F_o^2)^{\frac{1}{2}}$ | 0.037 | | 0.025 | 0.031 | | | 0.039 |
| $R_1$ (including $F_{hkl} = 0$) | 0.021 | | 0.035 | 0.069 | | | 0.083 |
| $F(000)$ | 324 | | 332 | 342 | | | 354 |
| $D_x$ [g/cm$^3$] | 3.170 | | 3.220 | 3.310 | | | 3.500 |
| $\mu$ (Mo$K\alpha$) [cm$^{-1}$] | 14.0 | | 19.3 | 27.7 | | | 43.0 |
| Approximate indices of boundary planes and their distance from an arbitrary origin [mm] | 110 0.0<br>$1\bar{1}\bar{1}$ 0.0<br>$\bar{1}1\bar{1}$ 0.0<br>$\bar{1}\bar{1}0$ 0.125<br>$1\bar{1}1$ 0.175<br>$\bar{1}11$ 0.225 | $\bar{1}10$ 0.038 | $11\bar{1}$ 0.0<br>$\bar{1}\bar{1}\bar{1}$ 0.0<br>$1\bar{1}0$ 0.0<br>$00\bar{1}$ 0.025<br>$\bar{1}10$ 0.062<br>110 0.088<br>111 0.157 | $\bar{1}10$ 0.0<br>110 0.0<br>001 0.0<br>$1\bar{1}0$ 0.125<br>$\bar{1}00$ 0.050 | | | $\bar{1}00$ 0.0<br>$0\bar{1}0$ 0.0<br>$00\bar{1}$ 0.0<br>100 0.10<br>010 0.025<br>001 0.125 |
| Crystal size [μm] | 120 × 60 × ca. 20 ± 3 and 83 × 40 × ca. 20 ± 3 | 191 × 115 × ca. 6 ± 2 and 300 × 127 × ca. 6 ± 2 | 155 × 148 × ca. 10 ± 3 | 200 × 125 × ca. 20 ± 3 | 70 × 35 × ca. 20 ± 3 | 19 × 17 × ca. 12 ± 3 | 140 × 140 × ca. 5.5 ± 2.0 and 98 × 70 × ca. 11.6 ± 1.4 |
| Orientation | ‖(100) and ‖(001) | ‖(100) and ‖(010) | ca. ‖(100) | ca. ‖(001) | | | ca. ‖(100) ‖(001) |
| | a | b | b | b | c | c | b |
| Effective diameter [μm] of entrance/exit apertures | 25/19.5 | 40.6/19.5 | 25/12.3 | 8/12.3 | 13/3.13 | 8/4.88 | 40.6/31.7 |
| Spectral band widths [cm$^{-1}$] | | | | | | | |
| $\tilde{\nu} \gtrsim 15000\,\text{cm}^{-1}$ | | | 100 cm$^{-1}$ | | | | |
| $\tilde{\nu} \lesssim 15000\,\text{cm}^{-1}$ | | | 300 cm$^{-1}$ | | | | |

[a] Polished crystals in araldite *E*
[b] Polished crystal fragments in araldite *E*
[c] Powder mount in canada balsam (*P*135) or glycerol (*P*150)

*Optical spectra*

Polarized single-crystal spectra in the range 35000 to 9000 $cm^{-1}$ were measured microspectrometrically (Langer and Abu-Eid, 1977). Data on crystal sizes and orientations, as well as measurement conditions, are given in Table 2. Crystal fragments of the Ultevis and Yakutian viridine were large and transparent and were easily oriented optically in the sample mounts prior to grinding and polishing. The kanonaite sample, on the other hand, was so deeply colored that optical orientation prior to grinding and polishing was impossible. Therefore, in such instances, fragments used for measurements were chosen according to their conoscopic picture and were close to the orientations given in Table 2. The synthetic samples were so fine grained that individual crystals could not be manipulated. In these cases the measurements were taken from grains which were found to be oriented between (100) and (110) as determined by morphology, character of elongation, and pleochroism. The spectra obtained were split into component bands of Gaussian shape by procedures described elsewhere (Abu-Eid et al., 1978). Several infrared spectra were recorded on powdered samples in order to check for the presence of OH in amounts larger than trace concentrations and to prove that no bands occur below 10000 $cm^{-1}$.

**Table 3.** Fractional atomic coordinates and thermal parameters (Å$^2$) with estimated standard deviations. The definition of the Debye-Waller temperature factor is $\exp -\frac{1}{4}(h^2 a^{*2} B_{11} + k^2 b^{*2} B_{22} + l^2 c^{*2} B_{33} + hka^* b^* B_{12} + hla^* c^* B_{13} + klb^* c^* B_{23})$, where $B_{13}$ and $B_{23}$ are zero for all atoms except O(4)

| Position | Parameter | ULT | TAN | DAR | KAN |
|---|---|---|---|---|---|
| $M1$ | | $Al_{0.920}$ $Mn_{0.023}$ $Fe_{0.057}$ | $Al_{0.756}$ $Mn_{0.182}$ $Fe_{0.062}$ | $Al_{0.562}$ $Mn_{0.342}$ $Fe_{0.096}$ | $Al_{0.302}$ $Mn_{0.680}$ $Fe_{0.018}$ |
| | $x/a$ | 0 | 0 | 0 | 0 |
| | $y/b$ | 0 | 0 | 0 | 0 |
| | $z/c$ | 0.2420(1) | 0.2425(1) | 0.2426(1) | 0.2429(2) |
| | $B_{11}$ | 0.57(3) | 0.68(2) | 0.73(3) | 0.59(2) |
| | $B_{22}$ | 0.30(3) | 0.40(2) | 0.51(2) | 0.41(2) |
| | $B_{33}$ | 0.26(3) | 0.32(2) | 0.38(2) | 0.00(2) |
| | $B_{12}$ | 0.12(2) | 0.12(1) | 0.08(2) | 0.12(2) |
| $M2$ | | $Al_{1.000}$ | $Al_{1.000}$ | $Al_{1.000}$ | $Al_{1.000}$ |
| | $x/a$ | 0.3707(1) | 0.3715(1) | 0.3724(1) | 0.3747(2) |
| | $y/b$ | 0.1387(1) | 0.1384(1) | 0.1379(1) | 0.1371(2) |
| | $z/c$ | 0.5 | 0.5 | 0.5 | 0.5 |
| | $B_{11}$ | 0.26 | 0.36(2) | 0.32(3) | 0.36(4) |
| | $B_{22}$ | 0.20(3) | 0.28(2) | 0.31(3) | 0.40(4) |
| | $B_{33}$ | 0.31(3) | 0.32(1) | 0.30(2) | 0.00(3) |
| | $B_{12}$ | 0.00(2) | 0.02(1) | 0.05(3) | 0.05(4) |

**Table 3.** (Continued)

| Position | Parameter | ULT | TAN | DAR | KAN |
|---|---|---|---|---|---|
| *T* | | $Si_{1.000}$ | $Si_{1.000}$ | $Si_{1.000}$ | $Si_{1.000}$ |
| | *x*/a | 0.2462(1) | 0.2469(1) | 0.2476(1) | 0.2491(2) |
| | *y*/b | 0.2523(1) | 0.2527(1) | 0.2534(1) | 0.2548(2) |
| | *z*/c | 0 | 0 | 0 | 0 |
| | $B_{11}$ | 0.26(3) | 0.41(2) | 0.46(3) | 0.46(3) |
| | $B_{22}$ | 0.17(3) | 0.26(2) | 0.36(3) | 0.38(3) |
| | $B_{33}$ | 0.30(3) | 0.31(1) | 0.39(2) | 0.05(3) |
| | $B_{12}$ | 0.01(2) | 0.03(1) | 0.08(2) | 0.08(3) |
| O(1) | *x*/*a* | 0.4231(3) | 0.4238(2) | 0.4248(3) | 0.4262(3) |
| | *y*/*b* | 0.3624(2) | 0.3628(1) | 0.3630(3) | 0.3624(3) |
| | *z*/*c* | 0.5 | 0.5 | 0.5 | 0.5 |
| | $B_{11}$ | 0.54(6) | 0.68(4) | 0.83(8) | 0.83(9) |
| | $B_{22}$ | 0.28(6) | 0.35(4) | 0.44(7) | 0.53(9) |
| | $B_{33}$ | 0.44(6) | 0.49(4) | 0.55(7) | 0.12(9) |
| | $B_{12}$ | −0.00(5) | 0.00(3) | 0.05(7) | −0.06(8) |
| O(2) | *x*/*a* | 0.4244(3) | 0.4245(2) | 0.4242(3) | 0.4238(3) |
| | *y*/*b* | 0.3623(2) | 0.3624(2) | 0.3626(3) | 0.3624(3) |
| | *z*/*c* | 0 | 0 | 0 | 0 |
| | $B_{11}$ | 0.42(6) | 0.51(4) | 0.54(8) | 0.52(9) |
| | $B_{22}$ | 0.42(6) | 0.59(4) | 0.75(7) | 0.79(9) |
| | $B_{33}$ | 0.44(6) | 0.50(3) | 0.58(7) | 0.15(9) |
| | $B_{12}$ | −0.08(5) | −0.08(4) | −0.02(7) | −0.07(8) |
| O(3) | *x*/*a* | 0.1026(2) | 0.1032(2) | 0.1032(3) | 0.1042(3) |
| | *y*/*b* | 0.3998(2) | 0.3996(2) | 0.3994(3) | 0.3988(3) |
| | *z*/*c* | 0 | 0 | 0 | 0 |
| | $B_{11}$ | 0.35(6) | 0.43(4) | 0.39(8) | 0.31(8) |
| | $B_{22}$ | 0.29(6) | 0.29(4) | 0.41(7) | 0.47(8) |
| | $B_{33}$ | 0.95(6) | 0.96(3) | 0.86(7) | 0.54(9) |
| | $B_{12}$ | −0.02(5) | 0.02(3) | −0.07(7) | +0.01(8) |
| O(4) | *x*/*a* | 0.2313(2) | 0.2339(1) | 0.2370(2) | 0.2432(2) |
| | *y*/*b* | 0.1348(2) | 0.1359(1) | 0.1377(2) | 0.1411(2) |
| | *z*/*c* | 0.2394(3) | 0.2391(2) | 0.2387(3) | 0.2386(3) |
| | $B_{11}$ | 0.53(5) | 0.73(3) | 0.93(6) | 0.90(6) |
| | $B_{22}$ | 0.42(5) | 0.55(3) | 0.63(5) | 0.61(6) |
| | $B_{33}$ | 0.37(5) | 0.41(2) | 0.49(5) | 0.21(6) |
| | $B_{12}$ | −0.06(3) | −0.01(2) | 0.07(4) | −0.02(4) |
| | $B_{13}$ | −0.09(4) | −0.11(2) | −0.10(5) | −0.11(6) |
| | $B_{23}$ | 0.09(4) | 0.07(2) | 0.03(5) | 0.08(6) |

## 3. Experimental results

Results of the structure refinement are summarized in Tables 3 and 4 which present the site populations, the final atomic coordinates, the thermal

**Table 4.** Interatomic angles and distances in andalusite (Burnham and Buerger, 1961), viridines, and kanonaite. Estimated standard deviations of angles are less than 0.2° and less than 0.0003 nm or 0.0004 nm for $M-O$ and $T-O$ or $O-O$ distances respectively

| Sample | AND[a] | | ULT | | TAN | | DAR | | KAN | |
|---|---|---|---|---|---|---|---|---|---|---|
| | (deg.) | (nm) | (deg.) | (nm) | (deg.) | (nm) | (deg.) | (nm) | (deg.) | (nm) |
| $M(1)-O(1)$ (2×) | | 0.1830 | | 0.1834 | | 0.1838 | | 0.1844 | | 0.1853 |
| $-O(2)$ (2×) | | 0.1891 | | 0.1898 | | 0.1901 | | 0.1909 | | 0.1918 |
| $-O(4)$ (2×) | | 0.2085 | | 0.2098 | | 0.2129 | | 0.2169 | | 0.2245 |
| Mean | | 0.1935 | | 0.1943 | | 0.1956 | | 0.1974 | | 0.2005 |
| $O(1)-O(1)$ | 85.2 | 0.2477 | 85.4 | 0.2487 | 85.1 | 0.2486 | 85.0 | 0.2490 | 85.2 | 0.2509 |
| $O(1)-O(2)$ (2×) | 178.1 | 0.3720 | 178.1 | 0.3731 | 178.3 | 0.3739 | 178.4 | 0.3752 | 178.5 | 0.3771 |
| $O(1)-O(2)$ (2×) | 96.7 | 0.2780 | 96.5 | 0.2785 | 96.6 | 0.2792 | 96.6 | 0.2802 | 96.2 | 0.2808 |
| $O(1)-O(4)$ (2×) | 88.5 | 0.2738 | 88.6 | 0.2752 | 88.5 | 0.2775 | 88.2 | 0.2803 | 87.9 | 0.2857 |
| $O(1)-O(4)$ (2×) | 90.8 | 0.2793 | 90.9 | 0.2808 | 90.8 | 0.2832 | 90.9 | 0.2869 | 91.2 | 0.2941 |
| $O(2)-O(2)$ | 81.5 | 0.2469 | 81.6 | 0.2479 | 81.7 | 0.2487 | 81.8 | 0.2500 | 82.4 | 0.2526 |
| $O(2)-O(4)$ (2×) | 91.6 | 0.2854 | 91.7 | 0.2871 | 91.7 | 0.2896 | 91.7 | 0.2931 | 91.6 | 0.2993 |
| $O(2)-O(4)$ (2×) | 89.1 | 0.2794 | 88.9 | 0.2802 | 89.1 | 0.2831 | 89.2 | 0.2870 | 89.3 | 0.2936 |
| $O(4)-O(4)$ | 179.0 | 0.4170 | 179.2 | 0.4197 | 179.0 | 0.4258 | 178.8 | 0.4339 | 178.8 | 0.4489 |
| $M(2)-O(1)$ | | 0.1816 | | 0.1817 | | 0.1829 | | 0.1845 | | 0.1860 |
| $-O(4)$ (2×) | | 0.1818 | | 0.1815 | | 0.1813 | | 0.1813 | | 0.1804 |
| $-O(3)$ | | 0.1843 | | 0.1837 | | 0.1842 | | 0.1846 | | 0.1849 |
| $-O(3)$ | | 0.1886 | | 0.1903 | | 0.1907 | | 0.1915 | | 0.1926 |
| Mean | | 0.1836 | | 0.1837 | | 0.1841 | | 0.1846 | | 0.1849 |

[a] Data from Burnham and Buerger (1961)

**Table 4.** (Continued)

| Sample | AND[a] | | ULT | | TAN | | DAR | | KAN | |
|---|---|---|---|---|---|---|---|---|---|---|
| | (deg.) | (nm) | (deg.) | (nm) | (deg.) | (nm) | (deg.) | (nm) | (deg.) | (nm) |
| O(1)–O(4) (2×) | 98.9 | 0.2760 | 98.7 | 0.2756 | 98.3 | 0.2755 | 97.7 | 0.2753 | 96.3 | 0.2730 |
| O(1)–O(3) | 86.9 | 0.2516 | 86.5 | 0.2505 | 86.5 | 0.2515 | 86.3 | 0.2525 | 86.3 | 0.2536 |
| O(1)–O(3) | 161.0 | 0.3650 | 160.7 | 0.3667 | 161.1 | 0.3685 | 161.3 | 0.3709 | 162.3 | 0.3741 |
| O(4)–O(4) | 105.9 | 0.2902 | 106.2 | 0.2903 | 106.9 | 0.2914 | 107.8 | 0.2928 | 109.0 | 0.2936 |
| O(4)–O(3) (2×) | 126.2 | 0.3265 | 126.1 | 0.3255 | 125.8 | 0.3255 | 125.6 | 0.3253 | 125.2 | 0.3243 |
| O(4)–O(3) (2×) | 92.5 | 0.2677 | 92.8 | 0.2693 | 92.9 | 0.2698 | 93.3 | 0.2712 | 93.9 | 0.2727 |
| O(3)–O(3) | 74.1 | 0.2247 | 74.2 | 0.2255 | 74.6 | 0.2273 | 74.9 | 0.2288 | 76.0 | 0.2325 |
| *T*–O(3) | | 0.1614 | | 0.1619 | | 0.1623 | | 0.1631 | | 0.1636 |
| –O(4) (2×) | | 0.1630 | | 0.1630 | | 0.1629 | | 0.1628 | | 0.1624 |
| –O(2) | | 0.1636 | | 0.1642 | | 0.1643 | | 0.1644 | | 0.1638 |
| Mean | | 0.1628 | | 0.1630 | | 0.1631 | | 0.1633 | | 0.1631 |
| O(3)–O(4) (2×) | 111.4 | 0.2680 | 111.2 | 0.2681 | 111.5 | 0.2687 | 111.7 | 0.2697 | 112.3 | 0.2707 |
| O(3)–O(2) | 101.4 | 0.2514 | 101.8 | 0.2531 | 102.0 | 0.2537 | 102.3 | 0.2550 | 102.9 | 0.2561 |
| O(4)–O(4) | 109.2 | 0.2657 | 109.8 | 0.2667 | 110.1 | 0.2671 | 110.5 | 0.2675 | 111.2 | 0.2679 |
| O(4)–O(2) (2×) | 111.7 | 0.2703 | 111.3 | 0.2701 | 110.8 | 0.2693 | 110.2 | 0.2683 | 108.8 | 0.2653 |
| *M*(1)–*M*(1) | | 0.2693 | | 0.2696 | | 0.2708 | | 0.2719 | | 0.2728 |
| –*M*(1) | | 0.2866 | | 0.2874 | | 0.2877 | | 0.2884 | | 0.2888 |
| *M*(2)–*M*(2) | | 0.2976 | | 0.2983 | | 0.2982 | | 0.2985 | | 0.2976 |

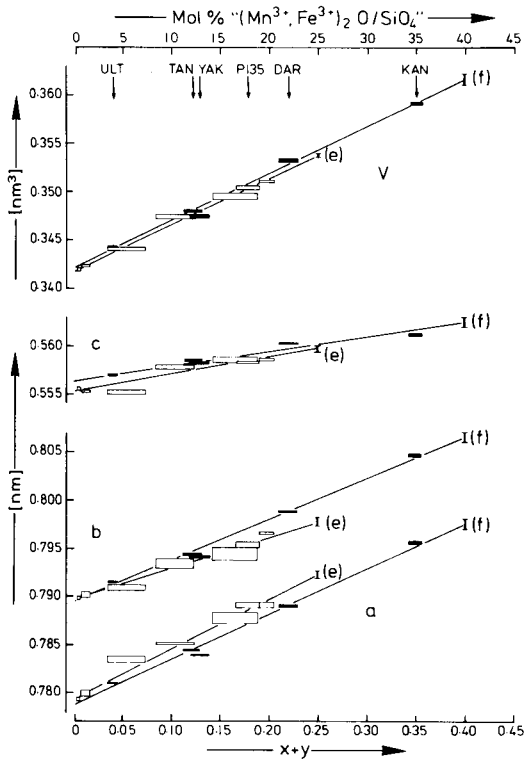


**Fig. 2.** Lattice constants of natural (closed symbols) and synthetic (open symbols) $(Al_{1-x-y}Mn_x^{3+}\ Fe_y^{3+})_2\ (O|SiO_4)$-minerals with andalusite structure as a function of substitutio-degree $(x+y)$. Samples of Table 1 are designated. Synthesis conditions of run products other than P135 and P150 will be published elsewhere (Abs-Wurmbach et al., in preparation). These synthetic viridiues are either single phase or EMP-analyzed samples. The size of the symbols refers to the uncertainties in composition and lattice constants, 1 s (cf. Table 1). The estimated standard deviations of the calculated regression curves are given as vertical bars

parameters, and the interatomic distances and angles, respectively. As will be discussed later, these properties change continuously with the concentration of Mn and Fe. The continuous changes also include the data obtained for the new mineral kanonaite. The present structure refinement of kanonaite confirms the first structural results of Vrana et al. (1977), who found $Mn^{3+}$ to substitute for Al in the octahedral $M1$ position. The continuous change of the lattice constants within the $(Al_{1-x-y}Mn_x^{3+}Fe_y^{3+})_2(O\,|\,SiO_4)$-series studied is evident from Figure 2. Single crystal data for natural samples and powder data for synthetic samples could be fitted by linear functions with slightly different coefficients ($r$ = correlation coefficient):

$$a_{\text{nat.[nm]}} = 0.0499\ (x+y) + 0.7784;\ r = 0.9969$$
$$a_{\text{syn.[nm]}} = 0.0516\ (x \qquad + 0.7793;\ r = 0.9972$$

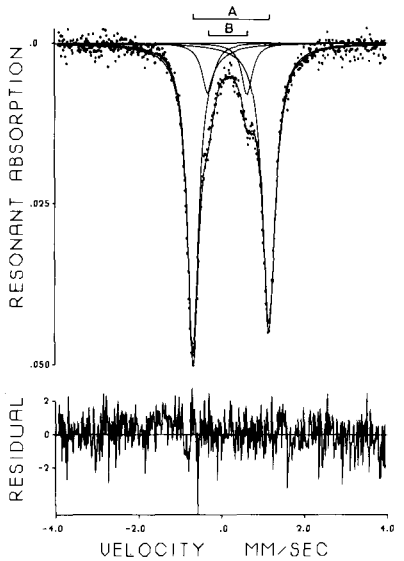


**Fig. 3**
Mössbauer spectrum of $^{57}Fe$ in the viridine from Yakutsk (Table 1: YAK) at room temperature. The abscissa gives the velocity relative to the $^{57}Co$ in Rh source. For conversion to metallic iron subtract 0.115 mm $s^{-1}$. The deviation of the solid line from the data (divided by the square root of the background) is plotted below the spectrum

$$b_{\text{nat.[nm]}} = 0.0456\ (x+y) + 0.7890;\ r = 0.9963$$
$$b_{\text{syn.[nm]}} = 0.0319\ x + 0.7898;\ r = 0.9906$$
$$c_{\text{nat.[nm]}} = 0.0152\ (x+y) + 0.5565;\ r = 0.9880$$
$$c_{\text{syn.[nm]}} = 0.0177\ x + 0.5553;\ r = 0.9889$$
$$V_{\text{nat.[nm}^3\text{]}} = 0.0519\ (x+y) + 0.3421;\ r = 0.9980$$
$$V_{\text{syn.[nm}^3\text{]}} = 0.0475\ x + 0.3418;\ r = 0.9997.$$

The slope of $a_{\text{syn.}}$ is less steep than that originally assumed on the basis of preliminary data on synthetic viridines (Abs-Wurmbach and Langer, 1975). In the earlier work only diffractometer data were available, whereas here the Guinier technique permitted inclusion of more reflections at higher $2\theta$ in the lattice constants refinement.

A typical Mössbauer spectrum and the hyperfine parameters obtained are presented in Figure 3 and Table 5, respectively.

Two doublets, $A$ and $B$, could be fitted under the spectral envelopes for the viridines from Yakutia and Tanzania. In the case of the Ultevis sample, there are also indications of the $B$ doublet. This doublet, however, is so weak that a four-band fit did not improve the value of $\chi^2$ significantly in unconstrained fits. The low isomer shifts $\delta$ of doublets $A$ and $B$ (Table 5) unambiguously demonstrate the trivalent state of iron. The fact that the quadruple splitting, $\Delta E_Q$, does not change with temperature (Table 5) is typical of high spin $Fe^{3+}$ (Bancroft et al., 1968). No doublet with parameters typical for $Fe^{2+}$ could be fitted. Therefore the $Fe^{2+}$ content, if any is present, is below approximately 4% of the total iron.

**Table 5.** Hyperfine parameters of $^{57}Fe$ in viridines from Ultevis or Yakutia and Tanzania based on two or four line fits, respectively

| Sample | ULT | YAK | | TAN |
|---|---|---|---|---|
| Absorber Temp. | 298 K | 77 K | 298 K | 298 K |
| Doublet A: | | | | |
| $T_L$ | 0.0160 | 0.0677 | 0.0486 | 0.0564 |
| $\Gamma_L$ | 0.357 | 0.351 | 0.438 | 0.392 |
| $T_H$ | 0.0109 | 0.0627 | 0.0438 | 0.0481 |
| $\Gamma_H$ | 0.401 | 0.400 | 0.377 | 0.460 |
| $\delta$ | 0.344 | 0.464 | 0.351 | 0.358 |
| $\Delta E_Q$ | 1.758 | 1.824 | 1.825 | 1.855 |
| Doublet B: | | | | |
| $T_L$ | | 0.0103 | 0.0068 | 0.0053 |
| $\Gamma_L$ | | 0.551 | 0.438 | 0.468 |
| $T_H$ | | 0.0100 | 0.0079 | 0.0059 |
| $\Gamma_H$ | | 0.389 | 0.357 | 0.507 |
| $\delta$ | | 0.346 | 0.269 | 0.295 |
| $\Delta E_Q$ | | 0.994 | 0.944 | 0.761 |
| $T_A/\Sigma T$ | | 0.865 | 0.863 | 0.904 |
| $F_A/\Sigma F$ | | 0.836 | 0.851 | 0.890 |

The indices $H$ and $L$ refer to the high and low velocity peaks, respectively.
$T$ Transmission,
$\Gamma$ fullwidth at half height (in $mm \cdot s^{-1}$),
$\Delta E_Q$ quadrupole splitting (in $mm \cdot s^{-1}$); uncertainty $\pm 0.01$,
$\delta$ isomer shift (in $mm \cdot s^{-1}$), relative to metallic iron, uncertainty $\pm 0.01$,
$F$ fractional area of the respective doublet

On the basis of recent work on hyperfine parameters of ferric iron in different coordination in silicate structures (Hafner and Huckenholz, 1971; Amthauer et al., 1976; Annersten and Hålenius, 1976) the range of isomer shifts, $\delta$, for $Fe^{3+}$ in four-fold coordination is $0.04-0.20$ mm $s^{-1}$ at 298 K relative to metallic iron, whereas $\delta$ for $Fe^{3+}$ in six-fold coordination ranges from 0.35 to 0.45 mm $s^{-1}$ at 298 K. Thus, the isomer shift of doublet $A$ (Table 5) is typical for octahedral ferric iron, whereas that of doublet $B$ is certainly larger than that expected for tetrahedral $Fe^{3+}$, but smaller than that for octahedral $Fe^{3+}$. Hence doublet $B$ is likely due to $Fe^{3+}$ in the five-coordinated $M2$ sites of the andalusite structure. From Table 5, it is obvious that 85 to 90% of the $Fe^{3+}$ substitutes for Al in the $M1$ octahedra of the andalusite structure, while the trigonal bipyramidal $M2$ sites contain only 10 to 15% $Fe^{3+}$. Expressed in terms of atoms per formula unit, $(Al_{1-x-y}Mn_x^{3+},Fe_y^{3+})_2\,(O|SiO_4)$, this means $2y = 0.008$ and 0.006 $Fe^{3+}$ in five coordinated sites in samples from Yakutia and Tanzania, respectively.

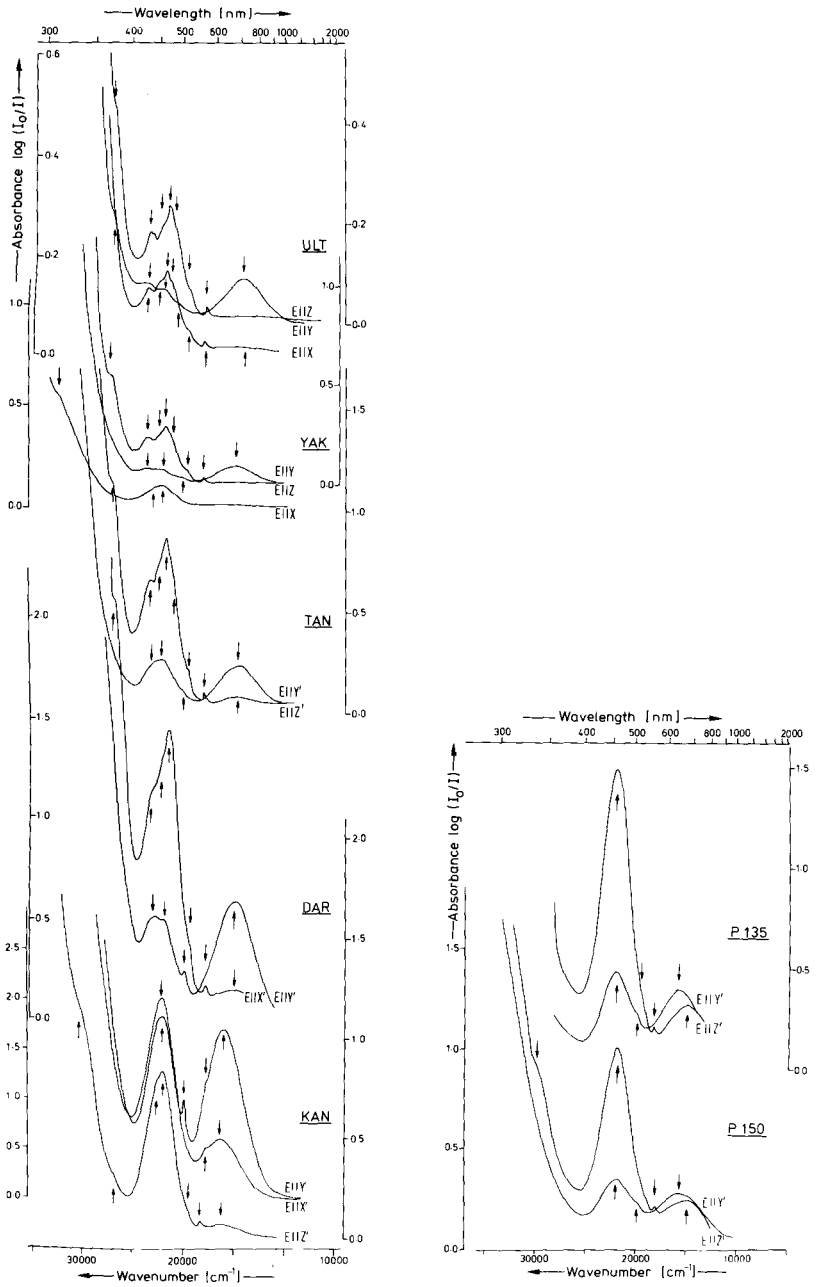


**Fig. 4.** Polarized optical absorption spectra of natural (left) and synthetic (right) $Mn^{3+}$-bearing andalusite type minerals (viridines and kanonaite). Spectra were recorded for the orientations $E \| X$, $Y$ or $Z$ in the sections: ULT (001), (100) or (100), resp.; YAK (010), (100) or (100), respectivity; KAN (001), (001), or ca. (100), respectivity

**Table 6.** Position of absorption maxima and shoulders in polarized spectra of natural and synthetic $Mn^{3+}Fe^{3+}$-substituted andalusite type minerals (viridines and kanonaite). Values are given in $cm^{-1}$

| Band No. | $E\|\|$[a] | ULT | YAK | TAN | DAR | *P*135 synthetic | *P*150 synthetic | KAN |
|---|---|---|---|---|---|---|---|---|
| 1 | *X* | nm | 32200 vst, sh | nm | nm | nm | nm | nm |
| | *Y* | nm | nm | nm | nm | nm | 34500 vst | nm |
| | *Z* | nm | nm | nm | nm | nm | 34000 vst | – |
| 2 | *X* | – | – | nm | 28500 vst | nm | nm | nm |
| | *Y* | – | – | – | 28500 vst | nm | – | – |
| | *Z* | – | – | 30000 ? vst | nm | nm | 29800 st, sh | 30200 st, sh |
| 3 | *X* | 26700 st, sh | – | nm | 26900 st, sh | nm | nm | – |
| | *Y* | – | – | – | – | – | – | – |
| | *Z* | 26800 st, sh | 27100 st, sh | 27000 st, sh | nm | – | – | 26800 m, sh |
| 4 | *X* | 23400 m | – | nm | 23300 m, sh | nm | nm | – |
| | *Y* | 23400 m | 23400 w | 23100 w, sh | 23100 m | – | – | – |
| | *Z* | 23300 m | 23500 m | nm | – | – | | 22500 st, sh |
| 5 | *X* | 22200 vw, sh | 22500 w, sh | nm | 22300 vw, sh | nm | nm | – |
| | *Y* | – | – | – | – | – | – | – |
| | *Z* | 22300 vw, sh | 22400 vw, sh | 22400 vw, sh | nm | – | – | – |

**Table 6.** (Continued)

| Band No. | $E\|\|$[a] | ULT | YAK | TAN | DAR | *P*135 synthetic | *P*150 synthetic | KAN |
|---|---|---|---|---|---|---|---|---|
| 6 | *X* | 21600 st | 2200 m | nm | 21600 st | nm | nm | 22100 st |
| | *Y* | 21800 m | 21900 m | 22100 m | 21800 m | 22000 m | 22000 m | 22000 m̄ |
| | *Z* | 21500 st | 21700 st | 21700 st | nm | 21900 st | 21900 st | 22000 st |
| 7 | *X* | 20900 w, sh | – | nm | – | nm | nm | – |
| | *Y* | 20700 vw, sh? | – | – | – | – | – | – |
| | *Z* | 20800 w, sh | 21000 w, sh | 20900 w, sh | nm | – | – | – |
| 8 | *X* | 19300 w, sh | – | nm | 19200 w, sh | nm | nm | – |
| | *Y* | – | 20100 w, sh | 20000 w, sh | 19800 vw | 19900 w, sh | 19800 w, sh | 19800 w |
| | *Z* | 19300 w, sh | 19500 w, sh | 19400 w, sh | nm | 19300 vw, sh? | ? | 19400 w, sh |
| 9 | *X* | 17800 vw | – | nm | 17700 vw | nm | nm | 17700 w, sh |
| | *Y* | – | – | – | – | – | – | 17600 vw, sh |
| | *Z* | 17750 vw | 17950 vw | 17950 vw | nm | 18180 vw | 18100 vw | 18250 vw |
| 10 | *X* | 14000 vw, b | – | nm | 15000 vw, b | nm | nm | 16300 w |
| | *Y* | 14100 m, b | 14700 m, b | 14600 m, b | 15000 m, b | 15800 m, b | 15700 m, b | 15900 m |
| | *Z* | – | – | 14600 vw, b | nm | 14900 w, b | 15000 w, b | 16200 vw, b |

Abbreviations: vst = very strong, st = strong, m = medium, w = weak, vw = very weak band, sh = shoulder, nm = no measurements in the respective range and/or polarization, horizontal bar = not observed, b = broad

[a] For deviations from the exact orientation cf. Table 2 and Figure 3

This interpretation of doublets $A$ and $B$ corresponds to that already proposed by Hålenius (1978), the hyperfine parameters $\delta$ and $\Delta E_Q$ for doublet $A$ in both Ultevis viridines being equal within the limits of error. Hålenius (1978), on the other hand, fitted doublet $B$ (11 % of the total resonant absorption) to the resonant absorption envelope of his Ultevis viridine and, in addition, a small doublet (7 % of the total resonant absorption) with parameters typical of octahedral $Fe^{2+}$. There were no indications of this doublet in our Mössbauer-spectra, although half widths of bands are a little smaller than those obtained by Hålenius (1978) and, hence, doublets $A$ and $B$ in the measured envelopes were more clearly discernable.

Polarized single-crystal spectra of natural and synthetic viridines and kanonaite are presented in Figure 4. The $E \| Y$ spectra of ULT and the $E \| Z$ spectra of YAK presented in Figure 4 are those taken from the (100) sections (cf. Table 2). The corresponding spectra taken from the (001) slice of ULT and the (010) slice of YAK, are not reproduced here, but exhibit the same shape. Positions and estimated intensities of absorption bands and shoulders, as taken from the spectra, are compiled in Table 6. Intensities and positions of the bands observed with the different orientations of the electrical vector $E$ explain the color and pleochroism of the viridines and kanonaite: the greenish-yellow color of $X$ and $Z$ is due to the intense absorption band centered at about 22000 $cm^{-1}$ and to the almost complete transparency below approximately 19000 $cm^{-1}$ in the $E \| X$ and $E \| Z$ spectra (Fig. 4). The emerald-green color of $Y$, on the other hand, is due to the minimum at around 19000 $cm^{-1}$ between the two bands centered at around 21700 and 15000 $cm^{-1}$.

The spectra of the Ultevis viridine in Figure 3 correspond in almost all details to those measured by Hålenius (1978) on another sample from Ultevis by means of conventional macroscale methods.

Small shoulders at about 27000, 22300, and 20900 $cm^{-1}$ (Fig. 3, Table 6) were not observed by Hålenius (1978), but were confirmed in the present work by repeated measurements. The band at 23400 $cm^{-1}$ (No. 4) which is present in all $E \| X$ spectra of natural samples, except kanonaite, was not found by Hålenius (1978) in his $\alpha$ spectrum. This may be due, at least in part, to the very high absorbance of the major band at 22000 $cm^{-1}$, which is near 2 in the paper cited.

A major difference between spectra of the synthetic andalusites containing $Mn^{3+}$ only and those of the natural samples containing ferric iron as well as $Mn^{3+}$, is that the former lack the fine structure of the strong band centered at about 21700 $cm^{-1}$. Hence the fine structure in the natural samples should be due, at least partially, to electronic transitions of $Fe^{3+}$ ions.

Examples for the results of the curve resolving procedure are presented in Figure 5. To resolve the spectra of the synthetic sample P150, two models, 1 and 2, have been applied which use one component band or two component bands to fit the strong absorption centered at 21700 $cm^{-1}$.

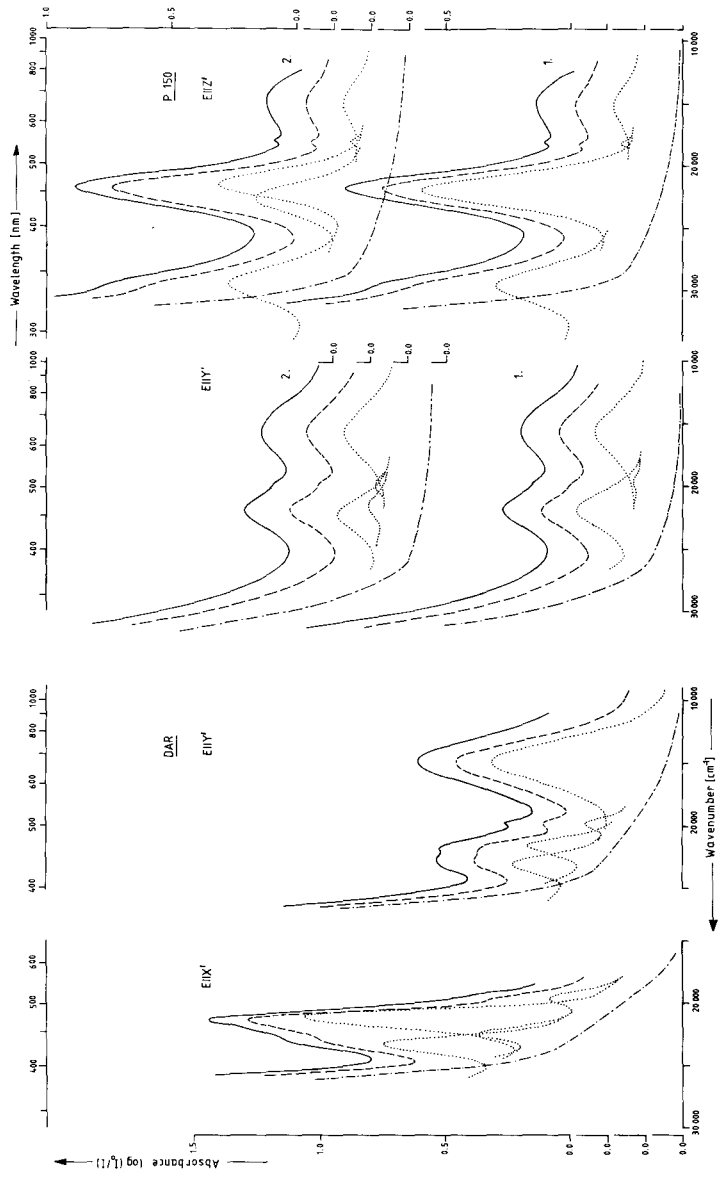


**Fig. 5.** Examples for band analyses of the optical spectra. Left: parts of the spectra of a natural $Mn^{3+}$, $Fe^{3+}$-substituted andalusite; right: spectra of a synthetic $Mn^{3+}$-substituted andalusite. In the latter case, two models for curve fitting process have been applied, 1 and 2. Solid line: observed spectra; dashed line: synthetic spectrum obtained as summation of the analyzed bands; dotted lines: analyzed component bands; dot-dashed lines: background. These individual curves were ordinate-shifted with respect to each other for the sake of clarity

The high-energy component band would correspond to the band or strong shoulder at about 23400 $cm^{-1}$ (No. 4, Table 6) in the natural samples. It is evident from Figure 5 that both models fit the observed envelope equally well.

The infrared spectra measured on some of the viridine samples did not show bands below 10000 $cm^{-1}$ down to approximately 1200 $cm^{-1}$ and, in this respect, correspond to andalusite spectra. The lattice vibrations below 1200 $cm^{-1}$ show slight band shifts to lower energies compared to those of pure andalusite. These spectra will not be discussed further in the present paper.

## 4. Discussion

The structure refinements were performed on the assumption that all manganese and iron occupies the octahedral positions $M1$ in the andalusite structure (cf. Table 3). The low $R$ values obtained on this assumption confirm this distribution model for the whole series of solid solutions between andalusite and kanonaite. This is independently confirmed for iron by the Mössbauer results, indicating a maximum of 10 to 15% of total iron is in the trigonal bipyramidal site $M2$. This distribution of transition elements in the whole mixed crystal series from andalusite to kanonaite confirms the first single-crystal X-ray data on kanonaite obtained by Vrana et al. (1978).

One half of the unit cell of kanonaite is shown in Figure 6, where the main structural changes within the solid solution series are also presented. The most prominent change is the elongation of the $M1$ octahedra, i.e., the increase of the $M1-O4$ distance by 7.7% in going from andalusite to kanonaite (Fig. 7). This octahedral distortion will play an important role in the interpretation of the optical spectra. It may be characterized by the octahedral $c/a$-ratio (Fig. 7), which demonstrates the type of distortion in this case more clearly than the bond-angle variance $\sigma^2$, and mean quadratic elongation, $\lambda$, or similar parameters, which were introduced by Robinson et al. (1971), Ghose and Tsang (1973), and Fleet (1976). The elongation leads to a tilting of both the $M2$ trigonal bipyramids and the Si tetrahedra (cf. Fig. 6). Concomitantly, the $M2-O1$ distances increase by 2.4% and the $M2-O3$ distances by 2.1%. The $M2-O4$ distances, on the other hand, decrease by 0.8%, which compensates partly for the elongations of $M2-O1$ and $M2-O3$, so that the mean $M2-O$ distances are nearly constant (+0.7%). This again reflects the very low fraction of $Mn^{3+}$ and $Fe^{3+}$ incorporated into these sites. The mean $M1-O$ distances, on the other hand, increase by 3.6%. These structural changes of the andalusite matrix in response to increasing manganese substitution may be compared with those obtained in a high-temperature crystal-chemistry study of the $Al_2SiO_5$ polymorphs by Winter and Ghose (1979). Within the 25 to 1000°C temperature range, the mean

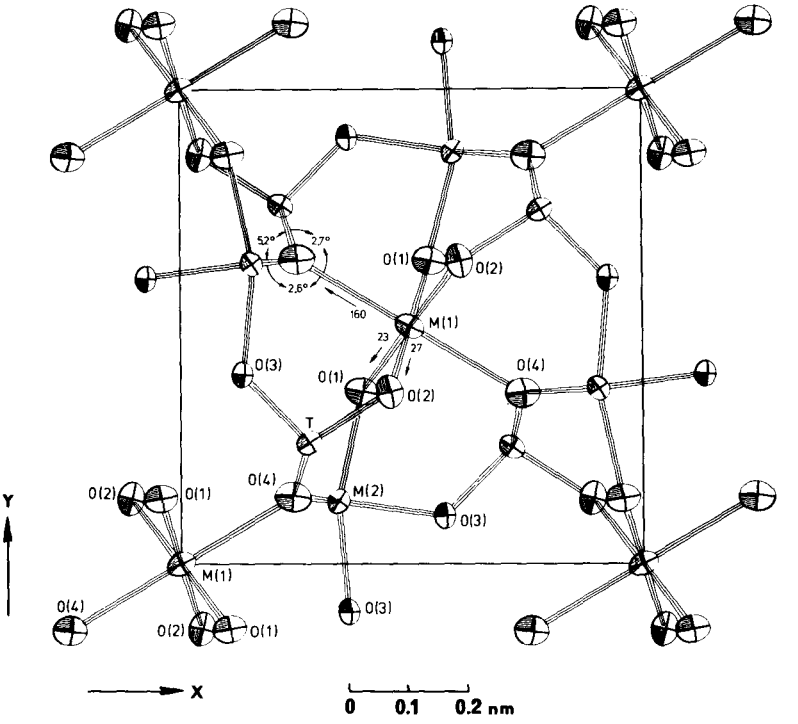


**Fig. 6.** Projection parallel [001] of the upper half of the unit cell of Kanonaite tilted clockwise by 10° around the $y$ axis to show the $M1-O$-octahedra more clearly. The shifts of oxygen atoms, coordinating the $M1$-position, as compared to their positions in andalusite, and the comcomitant changes of angles around O4 are given in $10^{-1}$ pm and degrees, respectively

$M1-O$ distances in andalusite increase by 1.4% and the mean $M2-O$ distances by 0.6%. This means, that the $M1-O$ octahedral expansion is about two times greater than the $M2-O$ expansion in the above temperature range, while this factor is approximately five in case of our mixed crystal series. As in the case of increasing $Mn^{3+}$-substitution, increasing temperatures influence most strongly the $M1-O4$ bond. Temperature was found to have no significant influence on the dimension and shape of the $Si-O$ tetrahedra (Winter and Ghose, 1979). Increasing substitution, on the other hand, slightly changes the tetrahedral shape, as is obvious from the 1.4% $T-O3$ increase (cf. Table 4), due to the tilting and distance changes in the $M2$ trigonal bipyramids. This observation is in agreement with the concept of structurally analogous variables (Hazen, 1977): substitution of Al by the larger $Mn^{3+}$ cation leads to similar structural changes as increasing temperature.

The structural changes discussed above are reflected by the behavior of the lattice constants. With increasing temperature or $Mn^{3+}$ substitution, $a$, $b$,

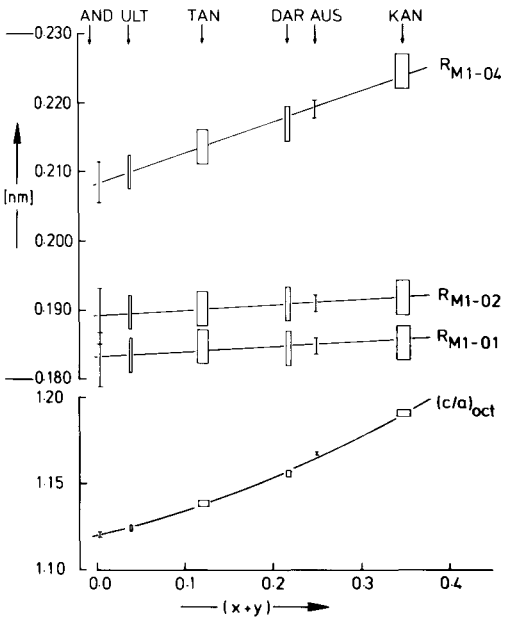


**Fig. 7.** $M1-O$ octahedral distances and the octahedral $(c/a)_{oct} = 2\,R_{M1O4}/(R_{M1O2} + R_{M1O1})$, in ($Mn^{3+}$, $Fe^{3+}$)-substituted andalusites. Note that the definition of $(c/a)_{oct}$ takes the $M1$-octahedra as tetragonal bipyramides, point group $D_{4h}$ (cf. Fig. 8). The data characterized by AUS were obtained from S. Hill (personal communication 1977)

and $c$ increase linearly, the slopes of the graphs decreasing in the order $a > b > c$. The slightly steeper slope of $a$ compared to $b$ can be interpreted in both cases by the fact that the $O4-M1-O4$ vector forms an angle of 30° with the [100] direction. The significantly smaller slope of $c$ with increasing temperature found by Winter and Ghose (1979) was attributed to chains of edge-connected $M1$ octahedra and fully extended chains of alternating Si tetrahedra and $M2$ trigonal bipyramids (interconnected by common corners with the octahderal chains) running parallel to [001] (see Fig. 9a of Burnham and Buerger, 1961). Winter and Ghose (1979) found that the bonds along [001] involved in the $Si-M2$-chain direction vary only slightly with temperature. The same is true for increasing substitution, because in this case the $M2$ trigonal bipyramids are almost free from $Mn^{3+}$ and $Fe^{3+}$. The linear regressions, given in section 3 for the dependence of $a$ and $b$ on the substitutional degree (Fig. 2), differ for the synthetic and natural minerals studied in this paper. The data for synthetic viridines converge more strongly than for the natural samples. The intersections of the curves, i.e., tetragonal cell metrics, occur at $x = 0.53$ (synthetic) and $(x + y) = 2.47$ (natural). The reason for this difference is not clear, but might be related to the presence of $Fe^{3+}$ in the natural samples.

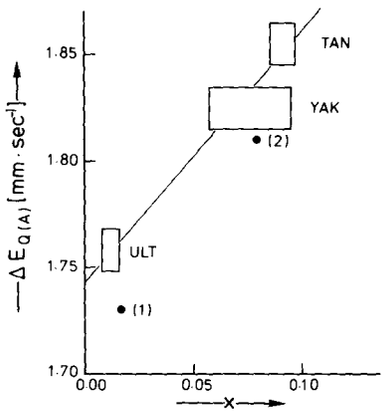


**Fig. 8**
Dependence of the room temperature quadrupol splitting of actahedral $^{57}Fe^{3+}$, $\Delta E_{Q(A)}$, in viridines as a function of the degree of the $Mn^{3+}$-substitution, $x$. Size of symbols represents the uncertainty limits. Points nos. (1) and (2) are for viridines from Ultevis and Vestanå, respectively, as measured by Hålenius (1978); no uncertainties were given for these values

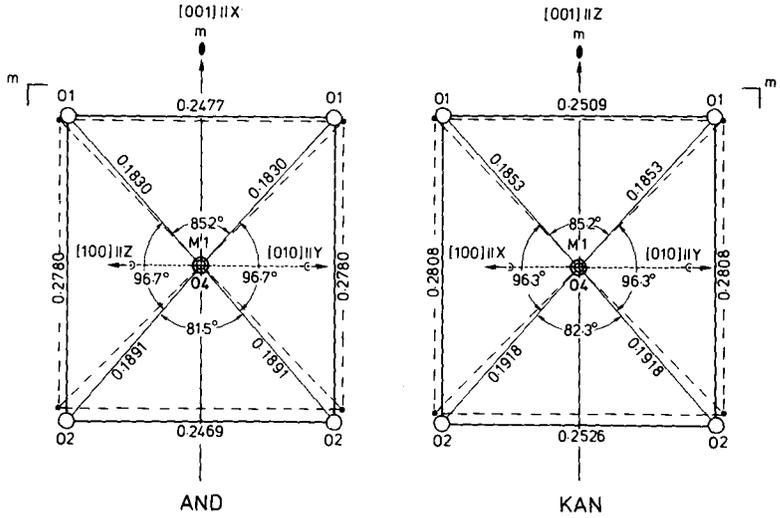


**Fig. 9.** ($M1O_6$)-octahedra in andalusite, AND, and the kanonaite studied, KAN, viewed along the octrahedral axis O4 – $M1$ – O4. Data for andalusite are from Burnham and Buerger (1961). The point symmetry of the octahedra is $C_{2v}$. The very small deviation of the O4$M$1O4 angle from 180° (cf. Table 4) is neglected. Dashed lines represent octahedra with undistorted octahedral planes of the same area as those of the distorted ones, i.e., octahedra with point symmetry $D_{4h}$. Note the small deviation of the octahedral planes from the ideal. The orientation of the refractive index indicatrix with axes $X$, $Y$, and $Z$ is also shown

Increasing distortion of the $M1$ octahedra with increasing manganese content of the andalusite mixed crystals $(Al_{1-x-y}Mn_x^{3+}Fe_y^{3+})_2(O|SiO_4)$ as discussed above is also reflected by the behavior of the $^{57}Fe^{3+}$ quadruple splitting, $\Delta E_Q$, with increasing $Mn^{3+}$ substitution $x$. Figure 8 shows that $\Delta E_Q$

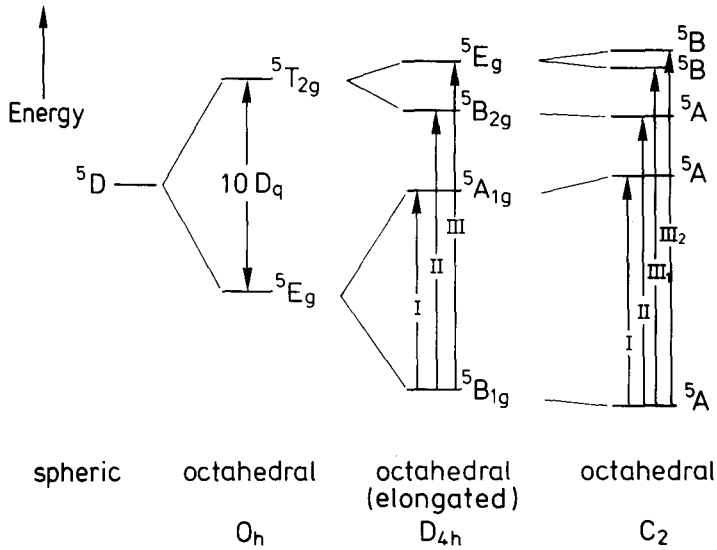


**Fig. 10.** Schematic energy level diagram for the splitting of the $^5D$ ground state of $M^{3+}$-ions in spheric and different octahedral fields: symmetry $O_h$, elongated octahedral $D_{4h}$, which are approximately realized in the $M1$-octahedra of the andalusite type mixed crystals (cf. Fig. 8), and $C2$, the true site symmetry of $M1$-sites in the structures studied (spin orbit coupling is neglected). Possible transitions are designated by Roman numbers

increases with $x$. The values of $\Delta E_Q$ obtained by Hålenius (1978) are also shown and follow the same trend. The extrapolation to $x = 0$, i.e., andalusite containing $Fe^{3+}$ but no $Mn^{3+}$, gives $\Delta E_Q = 1.74$ mm/s, an unusually high value when compared to other octahedral $Fe^{3+}$ values obtained for various mineral structures (Hafner and Huckenholz, 1971; Amthauer et al., 1976). This indicates the high degree of $M1$ distortion already present in $Mn^{3+}$-free andalusite.

In considering the assignment of the absorption bands in the optical spectra to $Mn^{3+}$ and $Fe^{3+}$ *dd* transitions the site symmetry of the $M1$ octahdedral positions (the relevant position according to the structural and Mössbauer results) is of prime importance. This position is the 4*e* site of space group *Pnnm*, with site symmetry of $C_2$. When isolating the octahedra from the surrounding structural matrix, their point symmetry may be taken as $C_{2v}$ as is evident from Figure 9. This figure shows further, that the distortion of the octahedral plane from a square arrangement is very small and, hence, the point symmetry may be approximated by $D_{4h}$ for the purpose of band assignment. The crystal field splitting of the spectroscopic $^5D$ ground state in isolate $Mn^{3+}$ -centered octahedra with point symmetries $O_h$, $D_{4h}$ (elongated) or $C_2$ is shown schematically in Figure 10. The splitting of the $^5E_g$ ground state would be expected on the basis of the Jahn-Teller (1937)

**Table 7.** Dependence of the absorption coefficients per cm, $k = \log (I_0/I)/t$, for the most intense bands in the $E \| Z$ and $E \| Y$ spectra on the degree of $Mn^{3+}$ substition $x$. Numbers in brackets are the errors

| Sample | | | ULT | YAK | TAN | DAR | *P*135 | *P*150 | KAN |
|---|---|---|---|---|---|---|---|---|---|
| $x$ | | | 0.012 | 0.076 | 0.091 | 0.171 | 0.173 | 0.22 | 0.340 |
| Band No. | Pos. | Pol. | | | | | | | |
| 6 | ~22000 | $E \| Z$ | 11(2) | 450(150) | 800(240) | | 658(99) | 671(168) | 1396(457) |
| 10 | ~15000 | $E \| Y$ | 35(5) | 133(44) | 172(52) | 231(35) | | | 958(80) |

theorem for the $3d^4$ configurated $Mn^{3+}$ ion. For the inferred point symmetry $D_{4h}$ of the elongated $Mn^{3+}O_6$ octahedra (cf. Figs. 6 and 7) we expect three spin-allowed transitions I, II, and III. As all transitions of the $3d^5$ $Fe^{3+}$ ion are spin-forbidden and because the $Fe^{3+}$ concentration is much lower than that of $Mn^{3+}$, except in the Ultevis sample (Table 1), the intensities of the bands originating from excitation of transitions I, II, and III in $Mn^{3+}$ should be higher by at least two orders of magnitude than those of $Fe^{3+}$. Further argument for the interpretation of the spectra is obtained from comparing the results on synthetic samples almost free of $Fe^{3+}$ with natural $Fe^{3+}$-bearing ones (Fig. 4). The strongest bands observed in synthetic and natural samples are those centered at 21800 $cm^{-1}$ and 15000 $cm^{-1}$ (Nos. 6 and 10 of Table 6) and are therefore attributed to spin-allowed $Mn^{3+}$ transitions. As there are no bands below 10000 $cm^{-1}$ down to the lattice-vibrational region, band No. 10 at 15000 $cm^{-1}$ is assigned to transition I and band No. 6 at 21800 $cm^{-1}$ to transition II. This assignment is further corroborated by the increase of the corresponding absorption coefficients, obtained directly from the spectra, with increasing $Mn^{3+}$ concentration (Table 7).

Identification of transiton III is difficult, as there is no third strong band in the spectra of synthetic viridines. In a preliminary note, Abs-Wurmbach et al. (1977) proposed two possibilities for the assignement of transition III:

a) the band or shoulder around 23300 $cm^{-1}$ in natural viridines (band No. 4 of Table 6),

b) the shoulder around 29000 $cm^{-1}$ in natural and synthetic viridines (band No. 2 of Table 6).

The difficulty with model *a* is that there is no corresponding band or shoulder in the spectra of synthetic viridines. If the model is correct, the band in question should then be hidden together with that originating from transition II under the strong envelope centered at 22000 $cm^{-1}$. However, this envelope has no asymmetry indicating such an overlap (Fig. 4). On the other hand, the envelope could be equally well fitted by either one or two Gaussian components (Fig. 5). A further difficulty with model *a* is that two

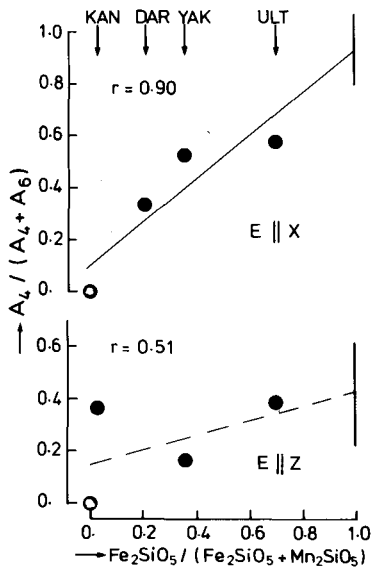


**Fig. 11**
Relative integral absorption coefficients $A$ (cf. Table 9) of band No. 4 at around 23300 $cm^{-1}$, as obtained by curve resolving, plotted against the '$Fe_2SiO_5$'-fraction. $r$ is the correlation coefficient. Note, that there is a positive correlation for $E||X$, whereas there is no correlation for $E||Z$. Opencircles represent $A_4/(A_4 + A_6) = 0$ to be expected for iron free viridine, if band 4 is exclusively due to $Fe^{3+}$-transitions (cf. Text)

relatively strong spin-forbidden $Fe^{3+}$ bands, derived from the ${}^6A_{1g} \rightarrow {}^4A_{1g}$, ${}^4E_g(G)$ transition in cubic fields are expected at about 23000 $cm^{-1}$ according to spectral results of Faye and Harris (1969) on andalusite, Faye and Nickel (1969) on kyanite, and Langer and Abu-Eid (1977) on acmite. These difficulties with model a forced Abs-Wurmbach et al. (1977) to propose model *b*.

Hålenius (1978), on the other hand, argued that the $Fe^{3+}$ concentrations are too low to account for the observed absorption coefficients of the 23300 $cm^{-1}$ band and, therefore, he favored model *a*. This interpretation was further corroborated by a calculation of the energy levels of the ($Mn^{3+}O_6$) cluster by the multiple scattering SCF-$X_\alpha$ method (Kai et al., 1980). These calculations proved the sequence of the crystal field split terms in Figure 10, and showed further that the energy difference between transitions II and III cannot be as large as required for model *b* [3].

If the 23300 $cm^{-1}$ band in question is due to $Fe^{3+}$ transitions, its intensity should correlate with the $Fe^{3+}$ concentration. Therefore, the integral absorption coefficient, $A = 1/d \int \ln (I_0/I)\, d\tilde{\nu}$, of band 4 was determined from curve resolved spectra and plotted, using the corresponding $A$ values of band No. 6 as internal standard, versus the Fe/(Fe + Mn) ratio of the samples. Figure 11 shows ambiguous results for the $E||Z$ spectra but a clear correlation between intensity and iron content for the $E||X$ spectra. From

[3] The values for transitions I, II, and III to be derived from the calculated energy level diagram cannot simply be regarded as the true absolute energy values of these transitions because of the necessary limitations in the model underlaying the calculations

**Table 8.** Half widths, $\Delta\tilde{\nu}_{1/2}$, absorption coefficients, $\alpha = \ln (I_0/I)/d$, integral absorption coefficients[a], $A = 1/d \int (I_0/I)/d\tilde{\nu}$, and assignments of resolved bands in the optical spectra. The individual band positions as obtained in the resolving procedure occur, within the limits of error, at the same energies as the

| Band No. (approx. position in $cm^{-1}$) | $E\|\|$ | ULT | | | YAK | | | DAR | | | $P$135 |
|---|---|---|---|---|---|---|---|---|---|---|---|
| | | $\Delta\tilde{\nu}_{1/2}$ [$cm^{-1}$] | $\alpha$ [$cm^{-1}$] | $A^a$ $10^{-4}$ [$cm^{-2}$] | $\Delta\tilde{\nu}_{1/2}$ [$cm^{-1}$] | $\alpha$ [$cm^{-1}$] | $A^a$ $10^{-4}$ [$cm^{-2}$] | $\Delta\tilde{\nu}_{1/2}$ [$cm^{-1}$] | $\alpha$ [$cm^{-1}$] | $A^a$ $10^{-4}$ [$cm^{-2}$] | $\Delta\tilde{\nu}_{1/2}$ [$cm^{-1}$] |
| 3 (26900) | $X$ | 800 | 50 | 10 | | – | | | na | | |
| | $Y$ | | – | | | – | | | – | | |
| | $Z$ | 1000 | 110 | 30 | 1400 | 650 | 90 | | nm | | |
| 4 (23300) | $X$ | 2100 | 100 | 50 | 2700 | 200 | 60 | 1700 | 675 | 110 | |
| | $Y$ | 2300 | 30 | 20 | 2300 | 155 | 30 | 1800 | 35 | 55 | 2600 |
| | $Z$ | 1600 | 120 | 45 | 1400 | 320 | 45 | | nm | | 2200 |
| 5 (22300) | $X$ | 800 | 60 | 11 | | na | | 1500 | 30 | 40 | |
| | $Y$ | – | – | – | | – | | | – | | |
| | $Z$ | 700 | 53 | 10 | | na | | | nm | | |
| 6 (21800) | $X$ | 1100 | 125 | 35 | 2100 | 230 | 55 | 1900 | 1200 | 220 | |
| | $Y$ | 1300 | 30 | 9 | 1600 | 135 | 20 | 1600 | 30 | 50 | 2800 |
| | $Z$ | 1400 | 215 | 75 | 2900 | 780 | 230 | | nm | | 2900 |
| 7 (20800) | $X$ | 700 | 40 | 8 | | – | | | – | | |
| | $Y$ | | – | | | – | | | – | | |
| | $Z$ | 1700 | 55 | 25 | 700 | 135 | 10 | | nm | | |
| 8 (19700) | $X$ | 2600 | 60 | 40 | | – | | 1500 | 20 | 25 | |
| | $Y$ | 1500 | 20 | 7 | 1400 | 60 | 15 | 1000 | 10 | 15 | 1400 |
| | $Z$ | 1700 | 55 | 20 | 800 | 140 | 8 | | nm | | |
| 9 (18000) | $X$ | 200 | 12 | 0.2[b] | | – | | 180 | 52 | 0.9[b] | |
| | $Y$ | | – | | | – | | | – | | |
| | $Z$ | 300 | 20 | 0.6[b] | 360 | 80 | 3[b] | | nm | | 240 |
| 10 (15000) | $X$ | | na | | | – | | | na | | |
| | $Y$ | 4400 | 95 | 110 | 5000 | 410 | 200 | 3800 | 590 | 300 | 3700 |
| | $Z$ | | – | | | – | | | nm | | 3500 |

[a] Integral absorption coefficients were derived from planimetrically measured areas of resolved bands
[b] Calculated: $A = \alpha \cdot \Delta\nu_{1/2}$

this, it can be concluded that there is at least a contribution of the above $Fe^{3+}$ transitions to the 23300 $cm^{-1}$ band (No. 4).

Therefore, in order to solve the discrepancies, it is proposed that both the $Mn^{3+}$ transition III and the above $Fe^{3+}$ transition contribute to the band at 23300 $cm^{-1}$ (No. 4). This assumption would also explain why, at relatively high Fe/(Fe + Mn) values (samples from Ultevis, Tanzania, and Yakutia), the 23300 $cm^{-1}$ band appears as a separate maximum (Fig. 4), while at low Fe/(Fe + Mn) values, at which the contribution of the $Fe^{3+}$ transition is only

absorption maxima and shoulders in the measured spectra themselves and, therefore, have been omitted here. sa and sf are spin-allowed or spin-forbidden transitions, respectively

| | | *P*150 | | | KAN | | | |
|---|---|---|---|---|---|---|---|---|
| α [$cm^{-1}$] | $A^a$ $10^{-4}$ [$cm^{-2}$] | $\Delta\tilde{\nu}_{1/2}$ [$cm^{-1}$] | α [$cm^{-1}$] | $A^a$ $10^{-4}$ [$cm^{-2}$] | $\Delta\tilde{\nu}_{1/2}$ [$cm^{-1}$] | α [$cm^{-1}$] | $A^a$ $10^{-4}$ [$cm^{-2}$] | |
| nm | | | nm | | | – | | |
| – | | | – | | | – | | $Fe^{3+}$ *dd-sf*: $^6A_{1g} \rightarrow [^4E_g(D)]$ |
| – | | | – | | 1400 | 230 | 33 | |
| nm | | | nm | | | – | | $Mn^{3+}$ *dd-sa*: $^5B_{1g} \rightarrow {}^5E_g(D)$ |
| 100 | 25 | 3100 | 335 | 110 | | – | | + $Fe^{3+}$ *dd-sf*: |
| 455 | 120 | 3200 | 790 | 215 | 1900 | 1600 | 330 | $^6A_{1g} \rightarrow [^4A_{1g}, {}^4E_g(G)]$ |
| nm | | | nm | | | – | | |
| – | | | – | | | – | | $Fe^{3+}$ *dd-sf*: $^6A_{1g} \rightarrow [^4A_{1g}, {}^4E_g(G)]$ |
| – | | | – | | | – | | |
| nm | | | nm | | | na | | |
| 340 | 100 | 1900 | 110 | 20 | | na | | $Mn^{3+}$ *dd-sa*: $^5B_{1g} \rightarrow {}^5B_{2g}(D)$ |
| 1220 | 340 | 2600 | 1010 | 280 | 2100 | 2580 | 600 | |
| nm | | | nm | | | – | | |
| – | | | – | | | – | | $Fe^{3+}$ *dd-sf*: $^6A_{1g} \rightarrow [^4T_{2g}(G)]$ |
| – | | | – | | | – | | |
| nm | | | nm | | | na | | $Mn^{3+}$ *dd-sf*: $^5B_{1g} \rightarrow [^3T_{1g}(H)]$ |
| 60 | 9 | 1300 | 90 | 12 | | na | | in natural samples: plus |
| – | | | – | | 1500 | 190 | 25 | $Fe^{3+}$ *dd-sf*: $^6A_{1g} \rightarrow [^4T_{2g}(G)]$ |
| nm | | | nm | | | na | | |
| – | | | – | | | na | | $Mn^{3+}$ *dd-sf*: $^5B_{1g} \rightarrow [^3T_{1g}(H)]$ |
| 35 | 0.8[b] | 300 | 38 | 1[b] | 400 | 115 | 5 | |
| nm | | | nm | | | na | | |
| 250 | 100 | 5000 | 360 | 180 | 3900 | 2650 | 1020 | $Mn^{3+}$ *dd-sa*: $^5B_{1g} \rightarrow {}^5A_{1g}(D)$ |
| 190 | 70 | 3200 | 130 | 50 | 3800 | 220 | 80 | |

[c] Excited terms in cornered brackets are those for the cubic case
nm = Not measured; na = not analyzed; – = band not present in this orientation and/or sample

small, this band appears as a shoulder (samples from Darmstadt and Kanona).

In Table 8, an assignment scheme for all resolved bands, Nos. 3 to 10 in natural and synthetic manganian andalusites is given. This scheme is based on the assigments of spin-allowed $Mn^{3+}$ transitions I, II, III just deduced, and on the spin-forbidden $Mn^{3+}$ transitions to be expected on the basis of the Tanabe-Sugano diagram (1954) for $3d^4$-configuration, as well as on $Fe^{3+}$ spin-forbidden transitions in octahedral position in silicates (Faye and

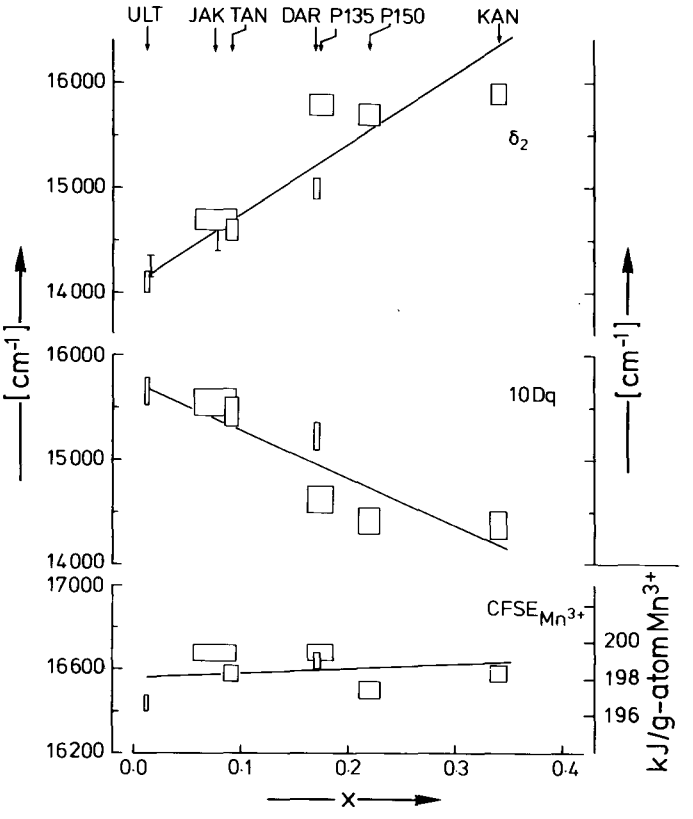


**Fig. 12.** $^5E_g$-ground state splitting of $Mn^{3+}$ (Jahn-Teller-splitting), $\delta_2$, crystal field parameter, 10 $Dq$, and crystal field stabilization energy of $Mn^{3+}$, $CFSE_{Mn^{3+}}$, in the andalusite structure type in dependence on the degree of the Al → $Mn^{3+}$ substitution, $x$. Simple bars represent data from Hålenius (1978). For the calculation of 10 $Dq$, the energies of transitions II and III (cf. Fig. 9) were taken from the $E \| Z$-spectra. $CFSE_{Mn^{3+}}$ was calculated on the basis of the band assignment in Table 9. 10 $Dq$ and $CFSE_{Mn^{3+}}$ for the synthetic samples, $P$135 and $P$150, were obtained by using energies for transitions II and III as obtained from curve resolution

Harris, 1969; Faye and Nickel, 1969; Moore and White, 1972; Langer and Abu-Eid, 1977). The half-height widths, $\Delta\tilde{\nu}_{1/2}$, absorption coefficients $\alpha$, and integral absorption coefficients $A$ are compatible with these assignements except for component band No. 8. In this case $\Delta\tilde{\nu}_{1/2}$ is too high for a normal spin-forbidden band. However, this may be due to difficulties of the curve resolution procedure (cf. resolved $E \| Y'$ spectra of DAR in Fig. 5). The bands, appearing as strong shoulders at around 33000 and 29000 $cm^{-1}$ (No. 1 and No. 2 of Table 6) may then be due to O – M charge transfer transitions, as no $dd$ transitions, additional to those of Table 8, are to be expected.

The assignment scheme and band energies of Table 8 have been used to calculate the crystal-field parameter 10 $Dq$ and the crystal field stabilization energy of $Mn^{3+}$ in andalusite octahedra. These properties are shown in Figure 12 as a function of the substitutional degree $x$ in the andalusite solid solution series, $(Al_{z-x-y}\, Mn_x^{3+}\, Fe_y^{3+})\,(O\,|\,SiO_4)$. The values of 10 $Dq$ and of the crystal-field stabilization energy, 15875 $cm^{-1}$ and 16650 $cm^{-1}$, respectively, obtained by Hålenius (1978) for a viridine sample from Ultevis with $x = 0.016$ and $y = 0.031$ are in accordance with those to be expected from the slopes in Figure 12. In addition to the crystal field parameter and crystal field stabilization energy, Figure 12 shows the ground-state splitting $\delta_2$ of $Mn^{3+}$ in the elongated octahedra. The increase of $\delta_2$ is due to the increasing elongation of the octahedra and compensates for the concomitant decrease of 10 $Dq$ so that the crystal-field stabilization energy of $Mn^{3+}$ is nearly independent of the manganese concentration.

*Acknowledgements.* S. Vrana (Prague) provided us with the kanonaite sample studied and D. M. Burt (Tempe), U. Hålenius (Luleå). D. S. Khorshinskii (Moscow), U. Kramm (Münster), K. D. Meinhold (Hannover), P. Paulitsch (Darmstadt), G. Roskamp (Mainz) and E. Seeliger† (Berlin), with viridine samples from different localities. S. Hill (Canberra) communicated unpublished structural results on a viridine from Central Australia. U. Hålenius (Luleå), P. B. Moore (Chicago), G. Smith (Berlin), and K. Weber (Berlin) read the manuscript critically and gave helpful comments. The Deutsche Forschungsgemeinschaft, Bonn-Bad Godesberg, provided financial support under grants No. Ki 166/1, La 324/3, 8, 10, Se 302/11.

To all these friends, collegues, and institutions our sincere thanks are due.

## References

Abraham, K., Schreyer, W.: Minerals of the viridine hornfels from Darmstadt, Germany. Contrib. Mineral. Petr. **49**, 1–20 (1975)

Abs-Wurmbach, I., Langer, K.: Synthetic $Mn^{3+}$-kyanite and viridine, $(Al_{2-x}Mn_x^{3+})\,SiO_5$, in the system $Al_2O_3-MnO-MnO_2-SiO_2$. Contrib. Mineral. Petr. **49**, 21–38 (1975)

Abs-Wurmbach, I., Langer, K., Tillmanns, E.: Structure and polarized spectra of $Mn^{3+}$-substituted andalusites (viridines). Naturwiss. **64**, 527 (1977)

Abs-Wurmbach, I., Langer, K., Schreyer, W.: Viridine, $(Al_{1-x}Mn_x^{3+})_2(O\,|\,SiO_4)$: its stability relations as a function of $P$, $T$, and $fO_2$. Proc. 11th Gen. Meeting IMA, Novosibirsk 1978, Vol. 9: Experimental Mineralogy (1980)

Abu-Eid, R. M., Langer, K., Seifert, F.: Optical absorption and Mössbauer spectra of purple and green yoderite, a kyanite related mineral. Phys. Chem. Mineral **3**, 271–289 (1978)

Amthauer, G., Annersten, H., Hafner, S. S.: The Mössbauer spectrum of $^{57}Fe$ in silicate garnets. Z. Kristallogr. **143**, 14–55 (1976)

Annersten, H., Hålenius, U.: Ion distribution in pink muscovite, a discussion. Am. Mineral. **61**, 1045–1050 (1976)

Bäckström, H.: Manganandalusit von Vestanå. Gerol. Fören. i Stockholm Förhandl. **18**, 386–389 (1896)

Bancroft, G. M., Burns, R. G., Stone, A. J.: Application of the Mössbauer effect to silicate mineralogy. – II. Iron silicates of unknown and complex structures. Geochim. Cosmochim. Acta **32**, 547–559 (1968)

Burnham, Ch. W., Buerger, M. J.: Refinement of the crystal structure of andalusite. Z. Kristallogr. **115**, 269–290 (1961)

Burnham, Ch. W.: Refinement of the crystal structure of sillimanite. Z. Kristallogr. **118**, 127–148 (1963a)

Burnham, Ch. W.: Refinement of the crystal structure of kyanite. Z. Kristallogr. **118**, 337–360 (1963b)

Chinner, G. A., Smith, J. V., Knowles, C. R.: Transition metal contents of $Al_2SiO_5$ polymorphs. Am. J. Sci., Schairer Vol. **267-A**, 96–113 (1969)

Corin, F.: Spectre d'absorption de la viridine. Bull. Soc. Geol. de Belgique **44**, 313–315 (1931)

Evans, H. T., Appleman, D. E. Handwerker, S. S.: The least squares refinement of crystal unit cells with powder diffraction data by automatic computer indexing method. Abstr., Am. Crystallogr. Assoc. Cambridge, Mass., Ann. Meet. Progr. 42–43 (1963)

Faye, G. H., Nickel, E. A.: On the origin of colour and pleochroism of kyanite. Can. Mineral. **10**, 35–46 (1969)

Faye, G. H., Harris, D. C.: On the origin of colour and pleochroism in andalusite from Brazil. Can. Mineral. **10**, 47–50 (1969)

Fleet, M. E.: Distortion parameters for coordination polyhedra. Mineral. Mag. **40**, 531–533 (1976)

Ghose, S., Tsang, T.: Structural dependence of quadruple coupling constant $e^2qQ/h$ for $^{27}Al$ and crystal field parameter D for $Fe^{3+}$ in aluminosilicates. Am. Mineral. **58**, 748–755 (1973)

Grapes, R. H., Hashimoto, S.: The Hidaka Viridine: a second look. J. Fac. Sci. Hokkaido Univ., Ser. IV, **17**, 602–612 (1977)

Hafner, S. S., Huckenholz, H. G.: Mössbauer spectrum of synthetic ferridiopsides. Nature Phys. Sci. **233**, 9–11 (1971)

Hålenius, U.: A spectroscopic investigation of manganian andalusite. Can. Mineral. **16**, 567–575 (1978)

Hazen, R. M.: Temperature, pressure and composition: structurally analogous variables. Phys. Chem. Mineral **1**, 83–94 (1977)

Heinrich, E. W., Corey, A. F.: Maganian andalusite from Kiawa Mountain, Rio Arriba County, New Mexico. Am. Mineral. **44**, 1261–1271 (1959)

Holuj, F., Thyer, J. R., Hedgecock, N. E.: ESR spectra of $Fe^{3+}$ in single crystals of andulusite. Can. J. Phys. **44**, 509–529 (1966)

Hamilton, W. C., Ibers, J. A.: International Tables for X-Ray Crystallography, Vol. IV., Kynoch Press, Birmingham 1974

Jahn, H. A., Teller, E.: Stability of polyatomic molecules in degenerate electronic states. I. Orbital degeneracy. Proc. Roy. Phys. Soc. (London) **A 161**, 220–235 (1937)

Kai, A. T., Larsson, S., Hålenius, U.: The electronic structure and absorption spectrum of manganian andalusite. Phys. Chem. Mineral, **6**, 77–84 (1980)

Klemm, G.: Über Viridin, eine Abart des Andalusites. Notizbl. Ver. Erdk. Darmstadt **32**, 4–13 (1911)

Kramm, U.: Chlorotoid Stability in Manganese Rich Low-Grade Metamorphic Rocks, Venn-Stavelot Massif, Ardennes. Contrib. Mineral. Petr. **41**, 179–196 (1973)

Kramm, U.: Kanonaite-rich viridines from the Venn Stavelot Massiv, Belgian Ardennes. Contrib. Mineral. Petr. **69**, 387–390 (1979)

Kulish, E. A.: Manganese-alumina rocks with Archean viridine in the Aldan shield. Geol. i. Geofiz., Akad. Nauk SSSR, Sibir. Otdel., No. **1**, 53–65 (1961)

Langer, K.: Synthetic 3 $d^{3+}$-transition metal bearing kyanites, $(Al_{2-x}M_x^{3+})SiO_5$. (Strens, R. G. J., ed.) The physics and chemistry of rocks and minerals, pp. 389–402. New York: Wiley 1976

Langer, K., Abu-Eid, R. M.: Measurement of the polarized absorption spectra of synthetic transition metal-bearing silicate microcrystals in the spectral range 44000–4000 $cm^{-1}$. Phys. Chem. Mineral **1**, 273–299 (1977)

Meinhold, K. D., Frisch, T.: Manganese – Silicate – Bearing Metamorphic Rocks from Central Tanzania. Schweiz. Mineral. Petr. Mitt. **50**, 493–507 (1970)

Moore, R. K., White, W. B.: Electronic spectra of transition metal ions in silicate garnets. Can. Mineral. **11**, 791–811 (1972)

Ödman, O. H.: Manganese mineralization in the Ultevis district, Jokkmokk, north Sweden. Part 2: mineralogical notes. Årsbok Sveriges Geol. Undersök **44**, No. 2 (Ser. C, Avh. Upps. no. 516) 28 pp (1950)

Okrusch, M., Evans, B. W.: Minor element relationships in coexisting andalusite and sillimanite. Lithos **3**, 261–268 (1970)

Prider, R. T.: Viridine from Mount Ragged, Western Australia. Indian Mineralogist **1**, 42–47 (1960)

Robinson, K., Gibbs, G. V., Ribbe, P. H.: Quadratic elongation: A quantitative measure of distortion in coordination polyhedra. Science **172**, 567–570 (1971)

Seifert, F., Olesch, M.: Mössbauer spectroscopy of grandidierite, $(Mg,Fe)Al_3BSiO_9$. Am. Mineral. **62**, 547–553 (1977)

Serdyuchenko, D. P.: Chemical composition and constitution of manganese andalusite (viridine). Zapiski Vsesoyuz. Mineral. Obshchestva **78** No. 2, 133–135 (1949)

Shabynin, L. I.: Viridine from S. Yakutia. Zapiski Vsesoyuz. Mineral. Obshchestva **77**, 203–214 (1948)

Smith, G., Strens, R. G. J.: Intervalence-transfer absorption in some silicate, oxide and phosphate minerals. (Strens, R. G. J., ed.) The physics and chemistry of minerals and rocks, pp. 583–612, New York: Wiley 1976

Strens, R. G. J.: Stability of $Al_2SiO_5$ solid solutions. Mineral Mag. **36**, 839–849 (1968)

Taylor, W. H.: The crystal structure of andalusite $Al_2SiO_5$. Z. Kristallogr. **71**, 205–218 (1929)

Tanabe, Y., Sugano, S.: On the absorption spectra of complex ions I. J. Phys. Soc. Jpn **9**, 753–766 (1954). On the absorption spectra of complex ions II, ibid. 766–779

Tillmanns, E., Gebert, W.: The crystal structure of tsumcorite, a new mineral from the Tsumeb Mine, S. W. Africa. Acta Crystallogr. **B29**, 2789–2794 (1973)

Vrana, S., Rieder, M., Podlaha, I.: Kanonaite, $(Mn^{3+}_{0.76}Al_{0.23}Fe^{3+}_{0.02})\,{}^{(6)}Al^{(5)}\,[O|SiO_4]$, a new mineral isotypic with andalusite. Contrib. Mineral. Petr. **66**, 325–332 (1975)

Winter, J. K., Ghose, S.: Thermal expansion and high-temperature crystal chemistry of the $Al_2SiO_5$ polymorphs. Am. Mineral **64**, 573–586 (1979)